University of Texas Rio Grande Valley
ScholarWorks @ UTRGV

Theses and Dissertations

7-2017

Removal of Lead and Arsenic from Aqueous Solution by Biochar Produced from Locally-Sourced Biomass

Sergio I. Mireles
The University of Texas Rio Grande Valley

Follow this and additional works at: https://scholarworks.utrgv.edu/etd

 Part of the Agriculture Commons, and the Environmental Sciences Commons

Recommended Citation

Mireles, Sergio I., "Removal of Lead and Arsenic from Aqueous Solution by Biochar Produced from Locally-Sourced Biomass" (2017). *Theses and Dissertations*. 288.
https://scholarworks.utrgv.edu/etd/288

This Thesis is brought to you for free and open access by ScholarWorks @ UTRGV. It has been accepted for inclusion in Theses and Dissertations by an authorized administrator of ScholarWorks @ UTRGV. For more information, please contact justin.white@utrgv.edu, william.flores01@utrgv.edu.

REMOVAL OF LEAD AND ARSENIC FROM AQUEOUS SOLUTION BY BIOCHAR PRODUCED FROM LOCALLY-SOURCED BIOMASS

A Thesis

by

SERGIO I. MIRELES

Submitted to the Graduate College of
The University of Texas Rio Grande Valley
In partial fulfillment of the requirements for the degree of

MASTER OF SCIENCE

July 2017

Major Subject: Agricultural, Environmental, and Sustainability Sciences

REMOVAL OF LEAD AND ARSENIC FROM AQUEOUS SOLUTION BY BIOCHAR PRODUCED FROM LOCALLY-SOURCED BIOMASS

A Thesis
by
SERGIO I. MIRELES

COMMITTEE MEMBERS

Dr. Jihoon Kang
Chair of Committee

Dr. Chu-Lin Cheng
Co-Chair

Dr. Jason Parsons
Committee Member

Dr. Tarek Trad
Committee Member

July 2017

Copyright 2017 Sergio I. Mireles

All Rights Reserved

ABSTRACT

Mireles, Sergio I. Removal Of Lead And Arsenic From Aqueous Solution By Biochar Produced From Locally-Sourced Biomass. Master of Science (MS), July, 2017, 84 pp., 3 tables, 14 figures

This study evaluated the effectiveness of four adsorbent materials, pyrolyzed corn stover, orange peel, pistachio shell, and magnetic biochar for their ability to adsorb lead (Pb) and arsenic (As III, As V) from aqueous solution. An increase in adsorption was seen as the pH of the solution increased from pH 2 to pH 6. Magnetic orange peel biochar with Fe_3O_4 particles precipitated on the surface of biochar was synthetized by co-precipitation and used for arsenic adsorption. Initial pH value had an influence on the adsorption behavior of As (III) and As (V). In the pH range of 2-6, As (V) adsorption was observed to decrease with increasing pH, with highest adsorption occurring at pH 2; As (III) adsorption had the highest capacity around pH 4-6.

DEDICATION

The completion of my master studies would not have been possible without the support and love of my family. My parents, Elizabeth Mireles, Sergio Mireles, and my sister Karen Mireles, who motivated me and supported me throughout this journey. I thank god for helping me get through this.

ACKNOWLEDGMENTS

I first give thanks to Dr. Jihoon Kang, my main advisor for all his help and advice over these past two years. I would also like to give thanks to my committee, Dr. Jason Parsons, Dr. Tarek Trad, Dr. Chu-Lin Cheng, and Dr. Anxiu Kuang for their support and advice.

I would like to give thanks to Dr. Juan Gonzalez, and Dr. James Hinthorne for their guidance and support. I also thank Mr. Tom Eubanks for helping me collect micrographs of my biochar samples. I also want extend my sincere gratitude to graduate students Diego Gonzalez, Jesus Cantu, Kenny Flores, and Carolina Valdes for helping my lab work.

TABLE OF CONTENTS

LIST OF TABLES

LIST OF FIGURES

CHAPTER I

LITERATURE REVIEW

1.1 Heavy Metals in the Environment

The term heavy metal is referred to any type of metallic element that has a relatively high density and is toxic at low concentrations. Heavy metals can essentially be described as a group of metals or metalloids with atomic densities greater than $4g/cm^{3,}$ or 5 times greater than the density of water (Nagajyoti et al., 2010). Many types of metals exhibit many types of oxidation states. Various names have been given to such subgroups including the transition metals (e.g. cadmium, zinc) and metalloids (e.g. arsenic and antimony). Heavy metals include lead (Pb), cadmium (Cd), nickel (Ni), cobalt (Co), iron (Fe), zinc (Zn), chromium (Cr), iron (Fe), arsenic (As), silver (Ag), and the platinum group elements.

Emission of heavy metals into the environment has been noted to occur throughout a wide range of different pathways, including air (e.g combustion), to surface water (e.g. runoff, transport), and to the soil (Jarup, 2003). Moreover, metals can be found naturally dispersed in geological formations, but urbanization and industrialization activities have increased the contribution of heavy metals in the biosphere. For example, industries such mining, smelting, and agricultural operations have contaminated large areas in the countries of Japan, Indonesia, and China by releasing metals such Cd, Cu, and Zn into agricultural lands, causing serious problems of soil contamination (Herawati et al., 2000).

Many reports have also released information regarding heavy metals in drinking water sources. In the state of Sonora, Mexico, drinking water from wells and storage tanks have been found to contain elevated levels of As, Cd, Cu, Hg, and Pb. The industrial, mining, and agriculture activities in the region have been attributed to contaminating such water resources (Chowdhury et al., 2016). The oxyanion, arsenic has also been found in great concentrations in the groundwater of the country of Bangladesh. It has been reported that nearly 60-75 million people are found to be at risk of arsenic exposure. Several factors have been attributed to this substantial input of arsenic in the environment of Bangladesh. This includes the constant usage of hazardous pesticides and chemical fertilizers in agricultural lands and the release of untreated effluents from facilities into bodies of water (Mukherjee and Bhattacharya, 2001).

1.1.1 Lead

Pb is a nonessential, highly toxic heavy metal, whose effects on biological systems are always of great concern in humans. Lead exists on both inorganic and organic forms and its physical and chemical properties greatly influence its distribution and behavior in the environment. (Hoffman et al., 2003). Lead contamination in the environment has been reported as being of great concern due to its toxicity to organisms and humans at low concentrations (Ding et al., 2014). The groups most susceptible to lead poisoning are fetuses and children. The effect of lead on the central nervous of children can be a serious health problem in adults and children. Chronic exposure to lead can lead to hyperactivity, irritability, headaches, and learning difficulties. To protect human health, the World Health Organization has set the allowable level of Pb at 10μg/L in drinking water systems (Sublet et al., 2003).

1.1.2 Arsenic

Element As has been shown to be abundant in the natural environment, in seawater and in the human body (Mohan and Pittman, 2007). Most of arsenic is mobilized by weathering processes, biological activities, geochemical reactions, and different types of anthropogenic sources. Environmental problems associated with arsenic exposure has been the result of mobilization under natural conditions. Although arsenic is naturally found in geological settings, different anthropogenic conditions such as mining activities, combustion of fossil fuels, and use of arsenic pesticides and herbicides have created additional impacts on the environment. Natural weathering processes have been estimated to release approximately 40,000 tons of arsenic to the global environment, while anthropogenic activities have released twice that amount (Thirunavukkarasu et al., 2001).

Arsenic exists in four stable oxidation states in the environment, which are arsenite (As III), arsenate (As V), arsenic (As 0) and arsine (As III) (Lorenzen et al.,1995). Among the four types of oxidation states of arsenic, the most common forms that exist in natural waters are arsenite (AsO_3^{3-}) and arsenate (AsO_4^{3-}), referred as Arsenic (III) and Arsenic (V). The slow redox transformations of arsenite and arsenate has made it possible for both arsenic species to be found in both reduced and oxidized environments. Under anoxic reducing conditions (e.g groundwater, sediments), arsenic exists as arsenite, whereas arsenate exists predominantly in aerobic oxidizing environments (e.g. surface waters) (Nicomel et al., 2016). As mentioned redox potential (Eh) and pH are the two major factors that control arsenic speciation. Under oxidizing conditions, $H_2AsO_4^-$ is the dominant species found at low pH values, while at higher pH, $HAsO_4^{2-}$ becomes the dominant species (Smedley and Kinniburgh, 2002). Moreover, the

uncharged arsenite species $H_3AsO^0_3$ becomes the dominant species at a pH less than 9.2. The speciation of arsenic as a function of pH is given in Fig 1.

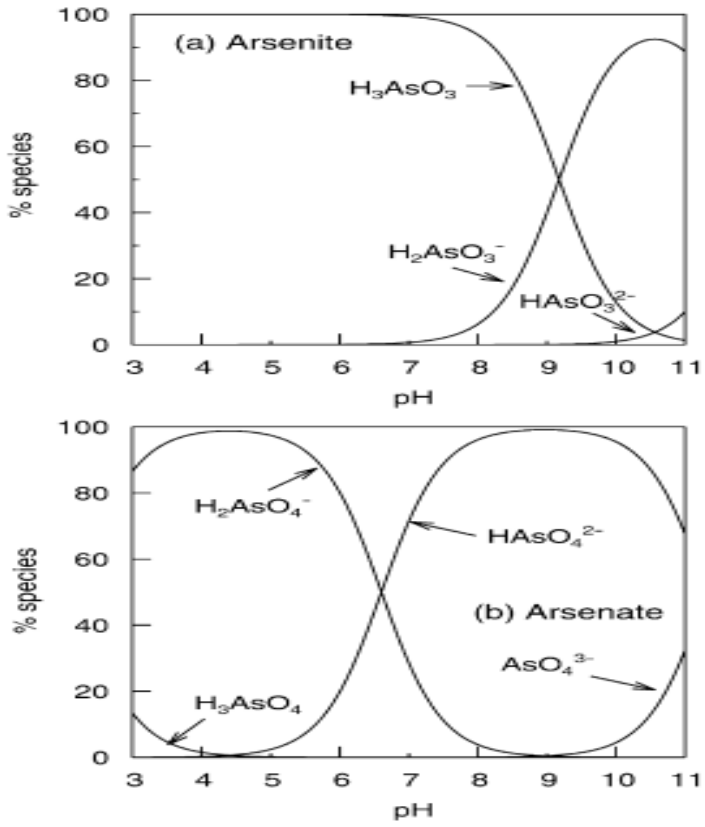

Figure 1. Speciation of As (III) and As (V) as a function of pH (Smedley and Kinniburgh, 2002)

Arsenic has been classified by the World Health Organization as a group 1 human carcinogenic substance (Nicomel et al., 2016). Ingestion of arsenic contaminated water has been reported to cause serious deleterious effects on the human body. Chronic intake of inorganic arsenic in present concentrations of above 50μg/L in drinking water can induce different types of skin lesions (e.g. hyperpigmentation) and cancers (e.g. skin, lung, kidney) in humans. Increased worldwide concern for the health effects of arsenic has promoted the World Health Organization to set the standard of 10μg/L in water. The current maximum contaminant level for arsenic in

drinking water is 50μg/L in the US (Thirunavukkarasu et al., 2001). Inorganic As (III) has been reported as being more toxic than As (V) to human health. The greater toxicity of As (III) is mainly due to its ability to be retained in the body longer since it becomes attached to sulfhydryl groups (Baird, 2003).

1.2 Adsorption

Adsorption is one of the many methods used to effectively remove contaminants. It is the process that occurs when liquid or gas accumulates in the interface of a solid or liquid. Lakherwal (2014) states that adsorption is highly effective in most natural, biological, and chemical systems, and used extensively in industrial applications for water purification. From the different methods used to remediate wastewater, adsorption is very suitable because of its simplicity and cost effectiveness (Yap et al., 2017).

Two main kinds of of adsorption processes occur: physical and chemical adsorption. Physical adsorption can occur on all surfaces of a material provided that optimal conditions like temperature and pressure are maintained. Furthermore, physical adsorption is the result of the interaction between the weak solid and gas interactions. Physical adsorption is the result of the weak Van der Waal's forces with adsorption energies not exceeding 80kJ/mole (Webb, 2003). Typically adsorbed molecules are diffused along the surface of the adsorbent material and are not bound to specific sites. Due to the weak bonding interactions between the adsorbate and the adsorbent, physical adsorption can easily be reversed.

Unlike physical adsorption, chemisorption is a very selective process and tends to occur only between certain types of adsorptive and adsorbent materials (Webb, 2003). Chemisorption tends only to proceed where there is a direct contact with the active sites on the adsorbent

material. Therefore, chemisorption is considered to be a single layer process. Both physical and chemical adsorption have been known to occur simultaneously at the surface of the adsorbent material.

1.2.1 Adsorption Isotherms

Knowledge of adsorption equilibria can be described mathematically using several adsorption models. The knowledge gathered from adsorption equilibrium data can form the basis of assessing the sorption potential of industrial sorbents. Each state of equilibrium is defined on several variables such as adsorbate concentrations, adsorbed amount, and temperature. A common process in equilibrium studies is to maintain the temperature constant and the express the equilibrium relationship in the form of adsorption isotherms (Worch, 2012). Several adsorption models have been used in the literature for the description of biochar equilibria with the Freundlich and Langmuir isotherm models being two of the most common.

The Langmuir adsorption isotherm is one of two most frequently used isotherm equations. The Langmuir isotherm can be expressed by the Equation 1

$$q = (S_{max} K_L C)/(1 + K_L C) \quad (1)$$

where

S_{max} is the maximum sorption capacity (mg kg^{-1}) and K_L is an affinity constant to bonding energy (L mg^{-1})

The above equation can be rearranged and linearized according to Equation 2

$$C/q = 1/(K_L S^{max}) + C/S^{max} \quad (2)$$

A linearized form of C/q against C yields the slope to be $1/S^{max}$ and the y -intercept equals $1/(K_L S^{max})$

The assumption of the Langmuir model is that:

- the molecules are adsorbed on a definite amount of active sites on the surface of the adsorbent
- each active site can only adsorb one molecule (monolayer)
- the surface of the adsorbent is uniform and all the sites are equivalent (Subbaiah, 2011)

The Freundlich adsorption isotherm is often used to express the variation of adsorption with concentration of adsorbate in solution at a constant temperature.

The Freundlich isotherm can be expressed by the Equation 3

$$q_e = K_F C_e^{1/n} \quad (3)$$

where C_e is the concentration of the adsorbate remaining in the solution, q_e is the mass of the adsorbate per unit mass of adsorbent and K_F and n are constants. The parameters can be determined in a linearized form of the Freundlich equation (4).

The linearized form of the equation is

$$\log q = \log K_F + 1/n \log C \quad (4)$$

where K_F is the measure of the adsorbent capacity. The plotted values of log q_e versus log C_e should give a linear regression with a slope of 1/n and a y-intercept of K_F. The n and K_F values can be calculated from the slope (Subbaiah, 2011).

1.3 Biochar

1.3.1 Background

Biochar has been defined as the solid remains of any type of organic material that has been heated in an oxygen free environment, with the objective of being applied to soil systems (Shackley et al., 2013). The discovery of biochar can be traced back to the 19th century, when European explorers in the Amazonas found dark patches of fertile soil among extremely weathered and acid oxisols in the region. These patches of fertile dark soils were referred as *terra preta* or dark soils and were created by the natives living in the region who blended biochar into the soil. The *terra preta* soils were high in carbon, with structures and microbial activity that enhanced nutrient availability and plant growth (Winsley, 2007) Furthermore, to distinguish between the terms charcoal and biochar, the difference ultimately lies between the end use of both carbon rich products. Charcoal is a source of charred organic material for producing fuel and energy, whereas biochar can be used for environmental management.

Biochar has also been recognized as a tool for combating climate change by sequestering carbon. This solid carbon rich material is produced through the process of pyrolysis. During the carbonization process of biomass, three main products of pyrolysis are achieved: bio-oil (liquid), syngas (gas), and biochar (solid). All of these products from the thermal degradation of biomass can influence the global carbon cycle in several ways. Galinato et al., (2011), states that all three materials can be used as an energy source that can replace fossil energy use. Second, if biochar is produced from a biomass (e.g rice husks, wood) that removes carbon from the atmosphere via photosynthesis, then char amended lands serve as a possible carbon sinks for long-term carbon storage.

Waste biomass has been widely used in the production of biochar, which includes: forest waste, crop residue, animal manure, municipal solid waste, and sewage sludge (Lyu et al., 2016). Although household or industrial waste can be generated into biochar, care has to be given to such products, since the solid C may contain traces of heavy metals and other types of organic pollutants that pose a threat to the environment. Many of forest and agricultural residue can be used to produce biochar, and in many cases these waste materials have little to no economic value Lehmann et al., (2006) has estimated that more than 50% of the total available residues in the U.S. can be acquired for less than $ 30 per ton of biomass. Most suitable feedstock materials for biochar production may include biomass that has high lignin concentrations yielding more quantities of biochar. Fig 2. demonstrates the different compositions and distinct thermal decompositions characteristics for three prime constituents in biomass: lignin, cellulose, and hemicellulose.

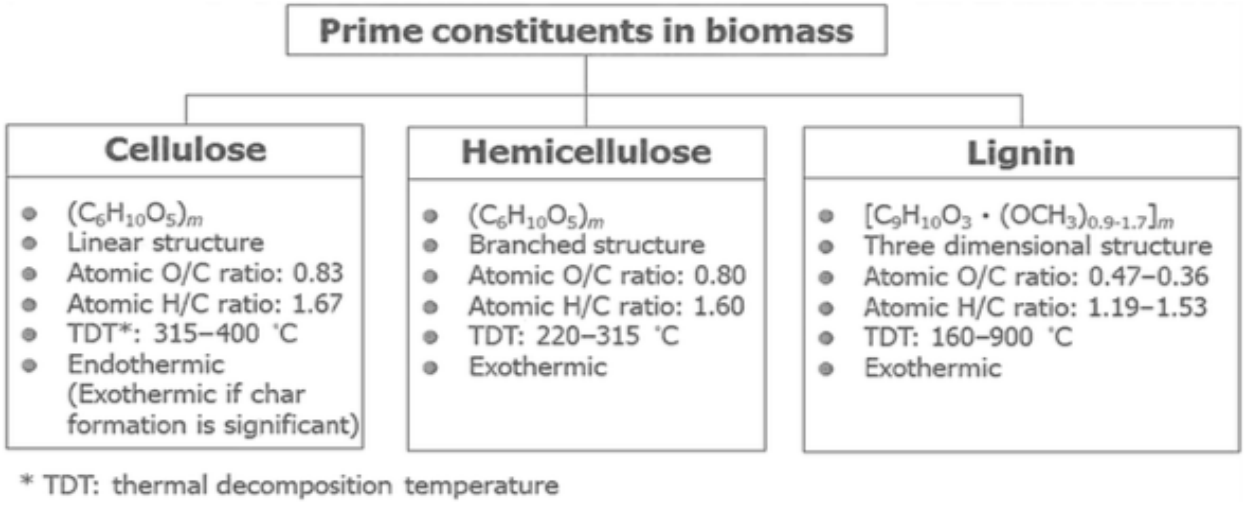

Figure 2. Chemical and thermal characterization of cellulose, hemicellulose, and lignin. (Chen, 2015)

Aside from biochar serving as an excellent material for soil fertility and carbon sequestration, environmental remediation has also been recognized as a new area where biochar can be applied (Ahmad et al., 2014). Different carbonaceous materials have long been used as sorbents for the removal of organic and inorganic materials in soil and water. Moreover, activated carbon its one of those carbonaceous materials that have been widely used in the treatment of water purification and has offered beneficial uses in human health. The term "activated" means that the charcoal has been treated with oxygen to increase the surface area and the micro porous structure of the material. Generally, the original material can be activated chemically by adding zinc chloride or by steam activation (Bandosz, 2006). Biochar is similar to activated carbon regarding the production process via pyrolysis and their medium to high surface areas. Nevertheless, biochar differs from activated carbon in that biochar does not have to be activated with chemicals or by steam activation. Yet, new research has focused on enhancing the sorption properties by impregnating iron oxide minerals onto the biochars surface.

1.3.2 Sorption Properties of Biochar

Biochar has been known to contain a non-carbonaceous area that can interact with several types of organic and inorganic contaminants (Ahmad et al., 2014). Furthermore, the oxygen containing functional groups on the biochar surface like the hydroxyl, carboxyl, and phenolic groups could effectively bind heavy metals, and many organic pollutants in water and soil systems. These sorption properties of biochar can be affected by several factors like pyrolysis temperature, residence time, and the type of biomass used for biochar production, which has a strong influence on way the material interacts with the contaminant. Hence, it is therefore critical to select the proper synthesis conditions for generating biochars.

As mentioned, surface chemical compositions contribute an important part in the adsorption properties of biochar. Fourier transformed infrared spectroscopy (FTIR) on different biochar has shown that surface functional groups tend to differ between different biomass materials and the synthesis temperatures in which the biochar is produced. (Kumar et al., 2011). Synthesis temperatures have been reported as having negative impact on the surface functional groups present on biochars, with higher temperatures decreasing most functional groups on the biochars surface. Cantrell et al., (2012), reported that most spectral features in manure biochar were lost at 700°C, except for some phosphate functional groups, leading the spectrum to resemble that of pure graphene. Aliphatics and aromatic amines were fully degraded in the biochars produced at 700°C along with the C=O associated with the carboxyl, ketones, and esters groups.

The solution pH is one of the most important factors that influence the adsorption process of many types of materials. The influence of pH on the adsorption process has been shown to be dependent on the type of biochar and the contaminant being removed (Tan et al., 2015). The biochar surface has been known to contain negatively charged functional groups (e.g. carboxyl, hydroxyl). Changes in solution pH has been reported to affect the behavior of the various oxygen containing groups of the biochars. At low pH values the functional groups become protonated due to an increase in hydrogen ions, which compete for the binding sites present on the biochars surface. Hence, electrostatic repulsion tends to occur between cations pollutants (e.g. Pb^{2+}, Zn^{2+}) and the positively charged biochar surface, thus lowering the adsorption process. An increase in pH has been reported to enhance the adsorption process of many heavy metals due to the deprotonation of the surface functional groups. Higher pH values decrease the competition

between the protons and the metal ions as more active sites on the biochars surface become available (Mohan et al., 2011).

Removal of heavy metals depends on the various biochar properties which includes surface functional groups, the medium to large surface areas, micro-porous structures, and mineral components. Possible adsorption mechanisms include several interactions like electrostatic attraction, ion exchange, physical adsorption, surface complexation, or precipitation (Tan et al., 2015). Mechanisms for the adsorption heavy metal lead and biochar have been described in the literature by Lu et al., (2012). Sewage sludge biochar was used to remove lead from acid mine drainage at several acid pH values. Lu et al., (2012) concluded that the removal of lead by the sewage-derived biochar occurred due to several types of removal mechanisms: 1) the metal was exchanged with K^+ and Na^+ due mainly to the electrostatic outer sphere complexation 2) exchange between Ca^{2+} and Mg^{2+}, which can be attributed to co-precipitation on the biochar surface with mineral oxides. 3) surface complexation between the carbonyl functional groups. 4) surface complexation between the interaction of the hydroxyl functional groups and lead ions.

CHAPTER II

REMOVAL OF LEAD FROM WATER BY BIOCHARS PRODUCED FROM AGRI-WASTE

2.1 Introduction

Heavy metal contamination can exist in discharge wastes from mining and smelting operations, energy and fuel production, fertilizer and pesticide industry, and metallurgical activities. Some of the metals associated with these activities include cadmium (Cd), chromium (Cr), lead (Pb), and mercury (Hg) (Bailey et al.,1999). Heavy metal ions are known to be stable and persistent in the environmental setting since they do not biodegrade easily and may be accumulated in organisms. If found in great concentrations, metal ions can cause harm to aquatic life and water reservoirs (e.g. groundwater, surface water) contaminated by toxic metals could pose a serious public health problem for human health (Demirbas, 2008).

Current techniques for heavy metal removal from water include adsorption, chemical precipitation, evaporation, use of ion exchange resins and membrane filtration (Agrafioti et al., 2014). Among these conventional techniques, adsorption is considered to be one of the most cost effective methods. Waste biosorbents, zeolites, and fly ash have been studied for remediating soil and water media contaminated from organic and inorganic contaminants (Saeed et al., 2005, Erdem et al., 2004, Bertocchi et al., 2006, Kobya et al., 2005). However, these adsorbents have been found to unfavorable to remove heavy metals due to some of their low sorption capacities

(Liu and Zhang, 2009). Recently there has been intense research regarding heavy metal removal using biochars in contaminated water and soil media and it has been found to perform well for heavy metals comparable to commercial activated carbon (Inyang et al., 2012).

Biochar is a carbon-rich solid material derived by heating biomass materials such as wood and manure in an oxygen-limited environment (pyrolysis or charring) which can be applied to soils for agricultural gains and carbon sequestration (Lehmann, 2007). The physicochemical properties of biochar, including medium to high surface areas, porous morphology, organic surface functional groups, and mineral composition also made it possible to use this material as an adsorbent for organic and inorganic contaminants in aqueous solutions (Tan et al., 2015). Biochar resembles some of the properties of activated carbon but it does not require an additional activation process that increases price and carbon footprint during manufacturing (Chun et al., 2004).

The goal of this study was to produce biochars from locally-sourced biomass and evaluate their efficacy for removing aqueous Pb. Among various metal ions present in wastewater, Pb is one of the most prevalent metal (Gupta and Rastogi, 2008). It is one of the toxic metals which accumulates mainly in bones, brain, kidney and muscles and exposure to high levels of lead can cause anaemia, encephalopathy, hepatitis and nephritic syndrome (Lo et al., 1999; Van der Perk, 2013). Thus, it is necessary to remove aqueous Pb from metal-contaminated water before discharge. Specific objectives of this study were to 1) produce biochar from three different feedstock materials at varying pyrolysis temperature (300°C, 450°C, and 600°C), 2) characterize the produced biochars including surface area, chemical functional group, and surface morphology, and 3) evaluate them as an adsorbent for removing aqueous Pb.

2.2 Materials and Methods

2.2.1 Production of Biochars

Three feedstock materials in this study were orange peel (OP), corn stover (CS), and pistachio shell (PS) (Fig. 3). OP was collected from a local grocery store in McAllen, Texas, USA while CS was collected off the outskirts of Pharr, Texas, just after the harvest of corn. PS were gathered from a local store where they were discarded as waste after the seed was extracted for food consumption. Collected OP and CS materials were washed three times with tap water for further use. The PS were submerged in tap water for 7 hours and then washed three times with tap water to remove residual salts. All materials were oven-dried at 105°C for 24 h, crushed using a coffee grinder, and screened through a 1-mm sieve. All materials were stored dry until further use.

Dry feedstock material (20g) was weighed to a quartz crucible and pyrolyzed under oxygen-limited conditions in a tube furnace (Lindberg/Blue M^{TM} 1100°C Tube Furnaces, ThermoFisher Scientific, Waltham, MA, USA). Prior to the pyrolysis of the biomass, the tube furnace was purged with nitrogen gas at a rate of 5 L min^{-1} for 45 minutes to remove the oxygen trapped inside the tube furnace. The CS, OP, and PS were pyrolyzed at 300°C, 450°C, and 600°C and held at the peak temperature for 1 h under 5 L min^{-1} of continuous nitrogen flow. The biochars are referred to as CS300, CS450, CS600, OP300, OP450, OP600, PS300, PS450, and PS600 in accordance with the pyrolysis temperature at 300°C, 450°C, and 600°C. Before removing the biochars from the furnace, they were cooled to 90°C inside the tube furnace under nitrogen flow to prevent rapid oxidation. All biochar samples were further ground and passed

through 250 μm sieves. Biochar yield was calculated by comparing biochar weight before and after pyrolysis in dry basis (Rehrah et al., 2014).

2.2.2 Characterization of Biochars

The pH and electrical conductivity (EC) of the biochars were measured in the extracts of (1:80 solid to solution ratio) after shaking the biochar materials with deionized (DI) water for 1 h. Moisture and ash content of the biochars were determined according to the Standard Test Method for Chemical Analysis of Wood (ASTM D1762-84). Surface functional groups on the surface of the biochars were examined by Attenuated Toral Reflectance Fourier transform infrared spectrophotometer (ATR-FTIR) which enabled samples to be examined without further preparation (Perkin Elmer., Waltham, MA, USA). The FTIR spectras were obtained at the 4000-650 cm^{-1} region and they were the average of 4 scans with a resolution of 4 cm^{-1}, which were used to characterize the functional groups based on their respective absorbance peaks.

Elemental compositions of the biochars were determined using SEM instrumentation equipped with energy dispersive X-ray spectroscopy (EDX). The EDX system works by categorizing emitted x rays based on the characteristic energy given by the sample (Chandler & Roberson , 2009)The samples were coated with an alloy of gold and palladium, mounted on metal stubs using a double stick tape. The metal coating of a gold/palladium was used to prevent buildup of high voltage charges on the biochar samples by conducting the charge to the ground. Surface area of biochar samples was determined by the Brunauer Emmett Teller (BET) multilayer adsorption method using a Quantachrome Nova 2200e instrument

2.2.3 Metal Adsorption Experiments

Single point adsorption test. Single point adsorption tests were conducted to determine top biochar materials for each feedstock type from varying pyrolysis temperature (300°C, 450°C, and 600°C). Briefly, a 250 ml of 10 mg Pb L^{-1} solution was prepared by diluting a stock solution (1,000 mg L^{-1}) that was made of lead nitrate ($Pb(NO_3)_2$) in DI water. Adsorption experiments were conducted in 5-ml polyethylene tubes containing 10 mg of the respective biochar materials with 4 ml aliquot of 10 mg Pb L^{-1}. The samples were shaken on a rotating shaker (Nutating Mixer, VWR International, Radnor, PA) for 1 h. Control samples containing mg Pb L^{-1} without biochar were included and all tests were done in triplicate. After 1-h equilibration, samples were centrifuged at 3,200 rpm for 5 min. The supernatant from each sample was collected and analyzed for Pb using Inductively coupled plasma optical emission spectroscopy (ICP-OES). The amount of Pb adsorbed by the biochar materials (q) was determined by:

$$q = (C_0V - CV)/M \quad [1]$$

where C_0 is the concentration of Pb in input solution (mg L^{-1}), V is the volume of liquid (L), C is the concentration of Pb in solution after 1-h equilibration, and M is dry weight of biochar (kg).

Effect of solution pH on lead adsorption. The effect of solution pH was determined over a pH range of 2-6 in triplicates. A Pb^{2+} solution was prepared at a concentration of 10 mg L^{-1} in DI water and pH adjusted to pH 2.0, 3.0, 4.0, 5.0, and 6.0 using either nitric acid or sodium hydroxide. All tests were conducted in 5-ml polyethylene tubes containing 10 mg of biochar with a 4 ml aliquot of 10 mg L^{-1} of Pb^{2+} at different pH (2-6). The polyethylene tubes were equilibrated for 1 h and followed identical procedures as in single point adsorption test.

Adsorption isotherms. The adsorption isotherm of Pb on biochar materials was conducted at varying concentrations of aqueous Pb (0, 5, 10, 25, 50, 100, and 250 mg L^{-1}) in triplicates and their initial solution pH was adjusted to pH 6, which found to be optimal pH for the aqueous Pb removal. Same ratio of biochar-solution ratio (10 mg of biochar in 4 mL of Pb solution) in the polyethylene tubes were equilibrated for 1 h and followed identical procedures as in single point adsorption test.

The Pb adsorption data were fitted using two macroscopic adsorption models, Langmuir and Freundlich. The Langmuir isotherm assumes monolayer adsorption of adsorbate (no stacking) on a homogenous surface of adsorbent while the Freundlich isotherm does not have this restriction (Tan et al., 2015). The Langmuir model is expressed by:

$$q = (S_{max} K_L C)/(1 + K_L C) \quad (2)$$

where S_{max} is the maximum sorption capacity (mg kg^{-1}) and K_L is an affinity constant to bonding energy (L mg^{-1}). Eq. (2) can be rearranged and linearized to:

$$C/q = 1/(K_L S^{max}) + C/S^{max} \quad (3)$$

A linearized form of C/q against C yields the slope to be $1/S_{max}$ and the y-intercept equals $1/(K_L S_{max})$.

The Freundlich model is expressed by:

$$q_e = K_f C_e^{1/n} \quad (4)$$

where K_F is the adsorption constant (mg kg^{-1}) and n is an empirical constant related to the intensity of adsorption (L kg^{-1}). These parameters were determined with a linearized form of the Freundlich equation:

$$\log q = \log K_F + 1/n \log C \quad (5)$$

A linear regression of log q against log C yields that the slope equals $1/n$ and the intercept equals log K_F.

2.3 Results and Discussions

2.3.1 Effect of Pyrolysis Temperature on Biochar Yield

Pyrolysis temperature was negatively correlated with biochar yield in all feedstock types. The temperature increase from 300°C to 600°C caused biochar yield to decrease from 43% to 29% for OS biochar, 37% to 25% for CS biochar, and 42% to 20% for PS biochar (Table 1). Our result is consistent with other studies (Yang et al., 2007; Cui et al., 2016; Kim et al., 2012) in that the negative correlation between pyrolysis temperature and biochar yield existed due to the decomposition of compounds such as cellulose, hemicellulose, and lignin as pyrolysis temperature increased. Yang et al. (2007) reported that these three main components in plant materials are affected by temperature with hemicellulose being easily degraded at 220-315°C, cellulose at 315-400°C, and lignin covered a whole temperature range of 150-900°C, which were gradually pyrolyzed with the increase of temperature in our study.

2.3.2 pH, EC, and Elemental Composition of Biochar

Raw feedstock materials have a pH of 6.5 to 6.8 but the pH values of biochars increased substantially as the pyrolysis temperature increased from 300 to 600°C for all biochar types (Table 1). The positive correlation between pyrolysis temperature and biochar pH was likely to be attributed to the generation of inorganic carbonates and alkaline salts in the ash fraction with increasing pyrolysis temperature (Yuan et al., 2011; Tan et al., 2014). Among three biochar

types, OP biochar showed the highest pH values (9.0-9.4) while PS biochars showed the lowest pH values (7.4-7.5). Mukome and Parikh (2015) noted that the non-wood feedstocks (e.g., algae, corn stover, grass, and manure) generally have higher pH than wood feedstock (e.g., nutshell, softwood, and hardwood), which is in agreement with our result.

EC is the ability of water to conduct an electrical current through dissolved salt ions. EC values of biochar materials increased with increasing pyrolysis temperature (Table 1). In general, biochar EC correlates more with feedstock type than pyrolysis temperature because it is a function of ash content and elemental composition, which are significantly affected by pyrolysis conditions and starring feedstock materials (Mukome and Parikh, 2015). In our study, OP biochars had the highest EC values (278-725 $\mu S\ cm^{-1}$) at all temperatures which were in line with their highest ash content (4.0-5.1 %) across feedstock types.

Carbon content of biochars determined from SEM-EDX increased with an increase in pyrolysis temperature, while the oxygen content as well as the O/C ratio decreased in all biochars with increasing pyrolysis temperature (Table 1). The increase in C indicated an increase in degree of carbonization with increasing pyrolysis temperature while the decline in O may be attributed to breakdown of O-based functional groups in biochar structure. The marked decreasing trend in O/C ratios at 600°C is likely due to the decline in polar functional groups resulting in the formation of aromatic structures in high temperature biochars (Zheng et al., 2013).

2.3.3 Surface Area of Biochars

The BET surface area is typically measured by assumed monolayer physical sorption of a gas (nitrogen gas N_2) onto the biochar surface at the temperature of liquid nitrogen (77K) (Mukome and Parikh, 2015). In this study, PS biochar had the greatest SA (279 m^2 g^{-1} at 600 °C) in all temperatures followed by OP and CS biochars (Table 1). The SA for PS and CS biochars were relatively low (< 5 m^2 g^{-1}). In general, there was positive correlation between surface area of biochars and pyrolysis temperatures. The breakdown of aliphatic bonds and phenolic groups in biochars and the gradual conversion to planar sheets of graphene may be responsible for the increase of SA as pyrolysis temperatures increased for CS and PS biochars (Zama et al., 2017). Above 600°C, non-carbon atoms are removed from lignocellulosic biomass and graphene sheets continue to grow laterally (Lechmann & Joseph, 2009). Exception was OP450 biochar which showed an opposite trend with its surface area less than OS300. This may be explained by the pores of biochars being eliminated or blocked by mineral ash, eventually leading to a decrease in overall surface area (Jin et al., 2016).

2.3.4 FTIR Analysis

The chemistry of biochar functional groups provides an understanding on the adsorption of heavy metals onto the biochars. FTIR spectra showed changes on the surface functional groups across feedstock types and different temperatures (Fig. 4) and our interpretations are based on several literatures (Keiluweit et al., 2010; Uchimiya et al., 2011; Ding et al., 2014). Several peaks were observed for low temperature CS biochar (CS300): 1) a peak at 2935 cm^{-1} corresponding to aliphatic C-H stretching; 2) a peak at ~1700 cm^{-1} corresponding to carboxyl

C=O streaching; 3) a peak at ~1587 cm^{-1} corresponding to aromatic C=C and C=O stretching of ketones and quinones; 4) a peak at ~1063 cm^{-1} indicating the presence of symmetric C-O stretching attributed to cellulose, hemicellulose, and lignin; 5) broad peak attributed to hydrogen bonded O-H stretching (3200-3500 cm^{-1}).

OP300 showed four distinct peaks in the region 2927-1000 cm^{-1}: 1) a peak at 2927 cm^{-1} corresponding to C-H_2 stretching; 2) a peak at 1696 cm^{-1} indicating C-O stretching for ester groups; 3) a peak at 1592 cm^{-1} related to N-H bend of amine groups; 4) a peak around 1000 cm^{-1} corresponding to Si-O stretching (Chen & Chen, 2009; Cantrell et al., 2012; Mary et al., 2016; Jindo et al., 2014). PS300 showed 1) –CH_2 stretching vibration at 2932 cm^{-1}; 2) an IR band at 1701 cm^{-1} indicative of C-O stretching; a peak at 1590 cm^{-1} indicating COO- asymmetric stretching; and a peak at 1100 cm^{-1} corresponding to –Si-O reactive groups (Jindo et al., 2014; Cantrell et al., 2012).

Noteworthy changes on the surface changes of biochars occur at 600°C for all biochar samples. For instance, between 450 and 600 °C (CS450 and CS600), all features related to water (O-H), oxygenated substituents (C=O and C-O), aliphatic C (C-H), and aromatic C=C streach progressively declined while new peaks appeared between 885 and 750 cm^{-1}, suggesting shift from being more aliphatic C-H to more aromatic C-H (Keiluweit et al., 2010). It was notable that the absorbance spectra of C-O stretch at 1063 cm^{-1}associated with hemicellulose, lignin, and cellulose decreased at 600°C. Features associated with oxygenated groups such as COO^-, C=O and C-O, progressively declined with an increase in pyrolysis temperature in all biochar samples. The Si-O spectra was observed on OP300 and PS600 and remained present at 600°C. Silica in known to be a fundamental component for plant phytoliths, which helps the plant from carbon degradation (Jindo et al., 2014)

2.3.5 Single Point Adsorption

The single point adsorption study was performed to determine optimal pyrolysis temperature for each feedstock type of biochars. The initial pH of the solution was 5.6 and no pH adjustment were made. Overall CS600 and OP300 performed the best in removing Pb more than 94 % compared to its initial concentration at 10 mg L^{-1} (Fig. 5). PS biochars were relatively poor in removing Pb. While increasing pyrolysis temperature improved Pb removal in CS and PS, OP biochars showed an opposite trend with OP300 being the most effective. Surface area analysis (Table 1) and FTIR spectras (Fig. 4) indicated that O-containing functional groups and surface areas played a significant role in adsorbing aqueous Pb. It was notable that higher Pb removal in the three biochars (CS600, OP300, and PS600) was tied to their surface area (i.e., higher surface area, greater Pb removal). Higher temperatures decreased some of the functional groups present for CS and PS biochars, but C-O, C=C, and COO- groups remained present on the surface of the biochars as shown in the FTIR spectras (Fig 4). Our result is in agreement with Ding et al. (2016) who reported that O-containing functional groups in woody type biochars may still remain at temperatures of 600°C. According to the results from single-point adsorption, CS600, OP300, and PS600 were selected for the remaining pH and isotherm experiments

2.3.6 Effect of Solution pH

Solution pH has been considered as one of the most significant factors in the adsorption of heavy metals onto different adsorbent materials (Zhou et al., 2017). The pH of the solution in our study significantly affected the adsorption of Pb onto the biochars. The adsorption capacity of each biochar increased with increasing pH (2-6) until it reached maximum adsorption at pH >

5 (Fig. 6). There were very limited Pb removal (< 1 %) at pH 2. Similar pH effects have been found in other studies. For instance, Li et al. (2016) reported that cadmium (Cd) adsorption capacity of *Eichornia crassipes* biochars increased as the solution pH increased from 3 to 6. In our study, the effect of solution pH was minimal for CS biochar accounting for 98, 98, and 96% of Pb removal at pH 4, 5, and 6, respectively. Overall our result could be explained by the surface charge of the biochars at different pH values. At a low pH, the surface of the biochars became protonated as the hydrogen ions bind to the negatively-charged sites in biochar. Hence, low adsorption occurred at low pH values due to the electrostatic repulsion between the positive surface of the biochar and the lead ions (Chen et al., 2011). As the pH of the solution increased, the surface functional groups of biochar became deprotonated, which resulted in higher Pb removal.

2.3.7 Adsorption Isotherms

The linearized form of the two adsorption models suggested that our data was better fitted using the Langmuir model than the Freundlich model (Table 2). The Langmuir model assumes that monolayer adsorption occurs on homogenous surface of the adsorbent material (Li et al., 2016). The poor linear fitting by the Freundlich model suggest that the supply of activate sites on the biochar surface was not infinite (Liu & Zhang, 2009). Our results are in agreement with Yap et al., 2017 who reported that the Langmuir model (R^2=0.98) was better fitted than the Freundlich model for the removal of Pb using coconut shell biochar. Langmuir adsorption model determined that S_{max} for Pb reached 25,000 mg kg^{-1} for CS600, 11,111 mg kg^{-1} for OP300 and 2,500 mg kg^{-1} for PS600 (Fig. 7)(Fig. 8).

Aqueous Pb adsorption on biochars was dependent on their physical and chemical properties resulting from the type of biomass and the pyrolysis temperature. Our data suggested that the O-containing functional groups on OP300 played an important role for the Pb sorption in OP biochar. The molar O/C ratio for OP300 was also the highest compared to the the other types of biomass materials (Table 1). These O-containing functional groups could possibly function as proton donors to remove Pb ions, by releasing H^+ from the surface to bind heavy metals (Xu et al., 2014). For high temperature biochars (CS600 and PS600), the presence of oxygen functional groups on the surface together with microporosity, and the exchange of ions between Pb and alkaline cations such as magnesium and calcium was likely to enhance Pb adsorption onto the biochars (Higashikawa et al., 2016). Komnitsas et al. (2015) found higher sorption capacities of Pb and Cu in pistachio shell biochars produced at 550°C. Although PS600 had a largest surface area compared to CS600 and OP300, its low performance for Pb removal could be due to a lack of active sites on the surface of the material, because PS is relatively carbon-rich biomass compared to CS and OP.

2.4 Conclusion

This study demonstrated that biochars produced from locally-sourced agricultural waste was effective in removing Pb from aqueous solutions. Based on our results, O-containing functional groups, irregular surfaces, and mineral contents on the biochars played an important role in removing aqueous Pb. The adsorption of Pb onto the biochars was influenced by the solution pH, with adsorption increasing as the pH of the solution increased. Isotherm adsorption data was well-fitted by the Langmuir isotherm model, suggesting Pb adsorption in this study was explained by monolayer adsorption of Pb onto the biochars. CS biochar was superior having its

S_{max} 2-10 times greater than OP and PS biochars, demonstrating its great potential as a filter media for Pb. The performance of OP300 was also notable as OP requires the least pyrolysis temperature (least energy input) and it is widely available in our region from intensive citrus farming. Future study using CS and OS biochars needs to examine Pb breakthrough under flowing condition for real-world applications as a filter media.

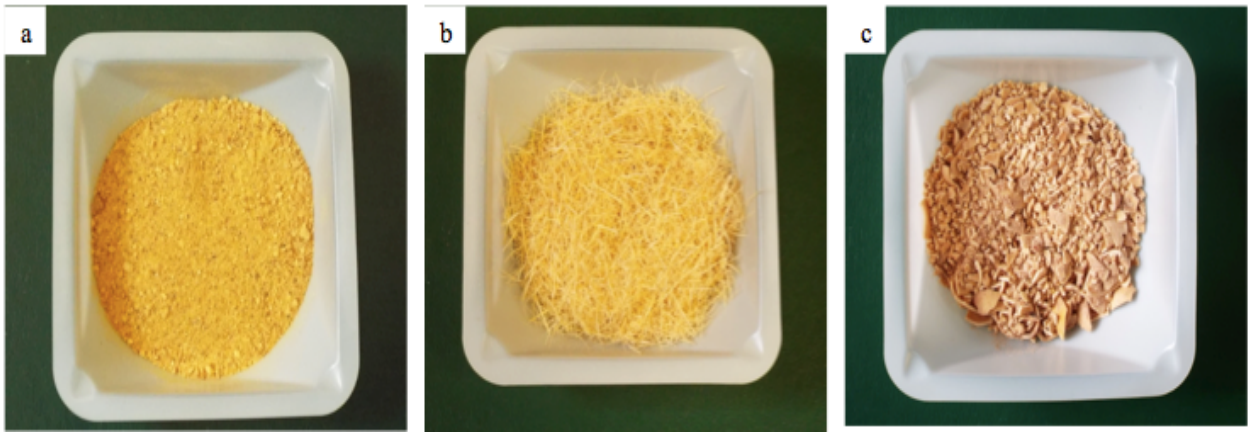

Figure 3. Biomass used for biochar production. (a) orange peel (b) corn stover (c) pistachio shells

A

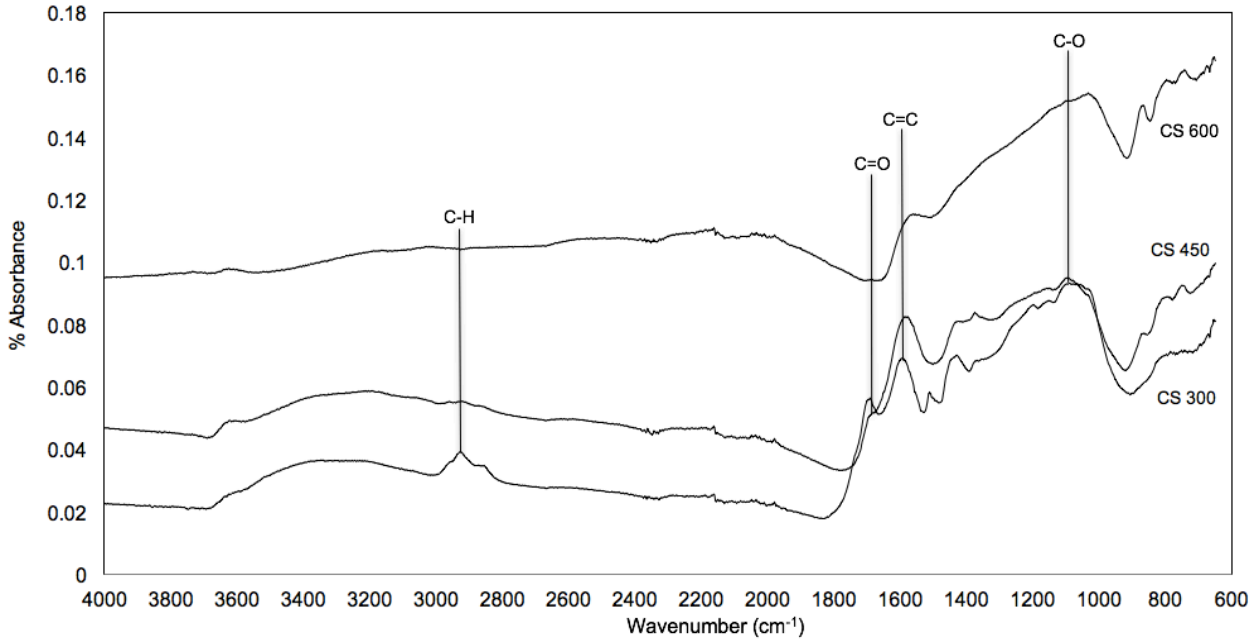

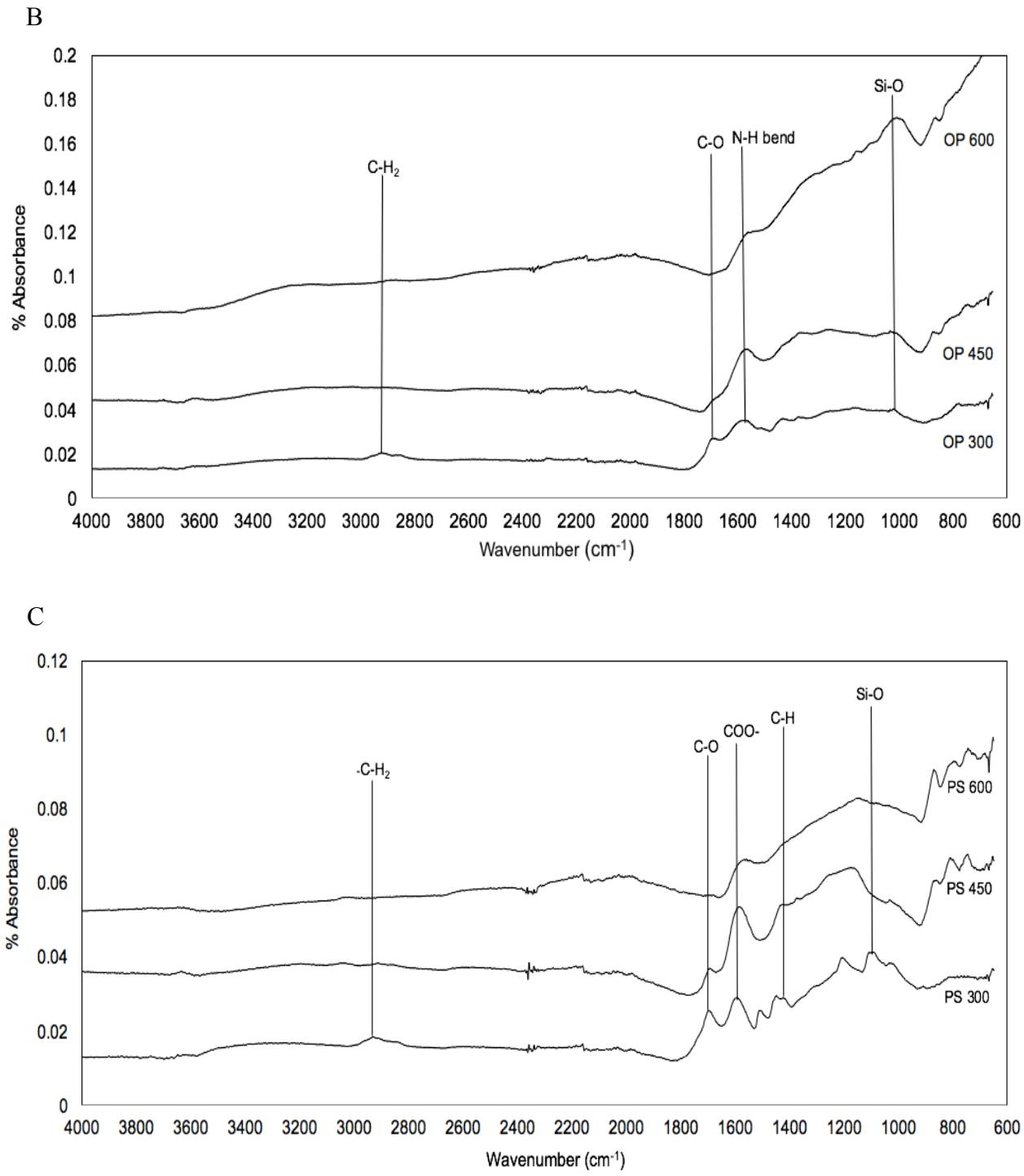

Figure 4. Fourier transform infrared (FTIR) spectra of different biochar samples. FTIR spectrum of (A) corn stover biochar; (B) orange peel biochars; (C) pistachio shell biochars

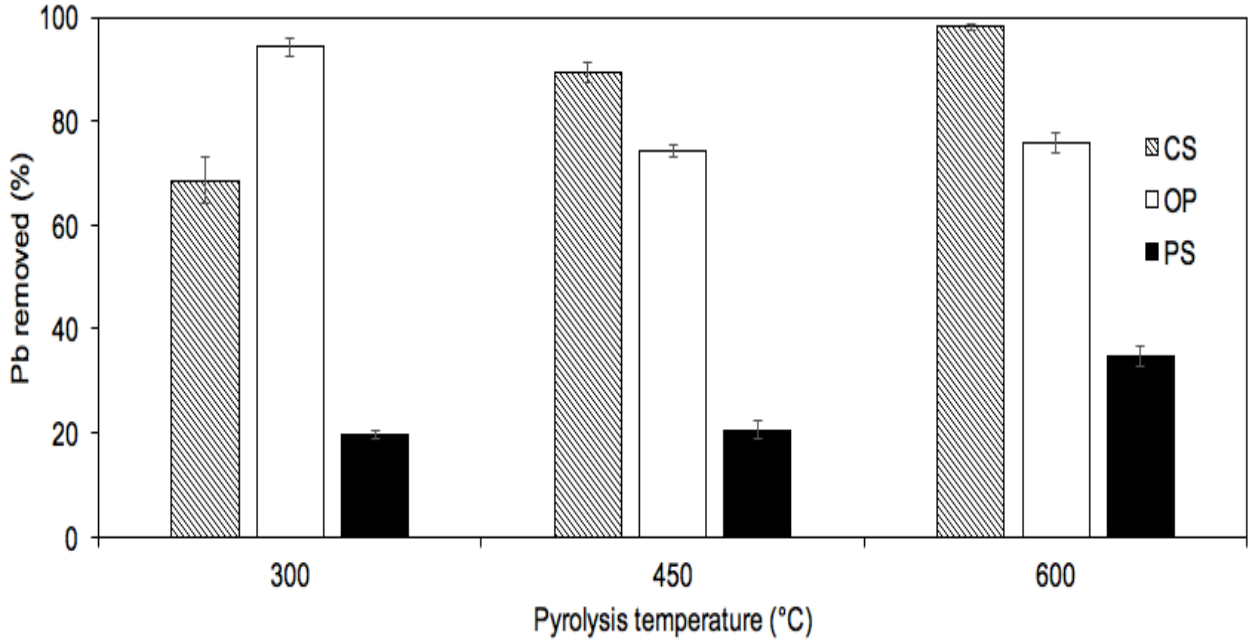

Figure 5. Adsorption of aqueous lead (Pb^{2+}) affected by pyrolysis temperature in each of the feedstock materials: corn stover (CS), orange peel (OP), and pistachio shell (PS).

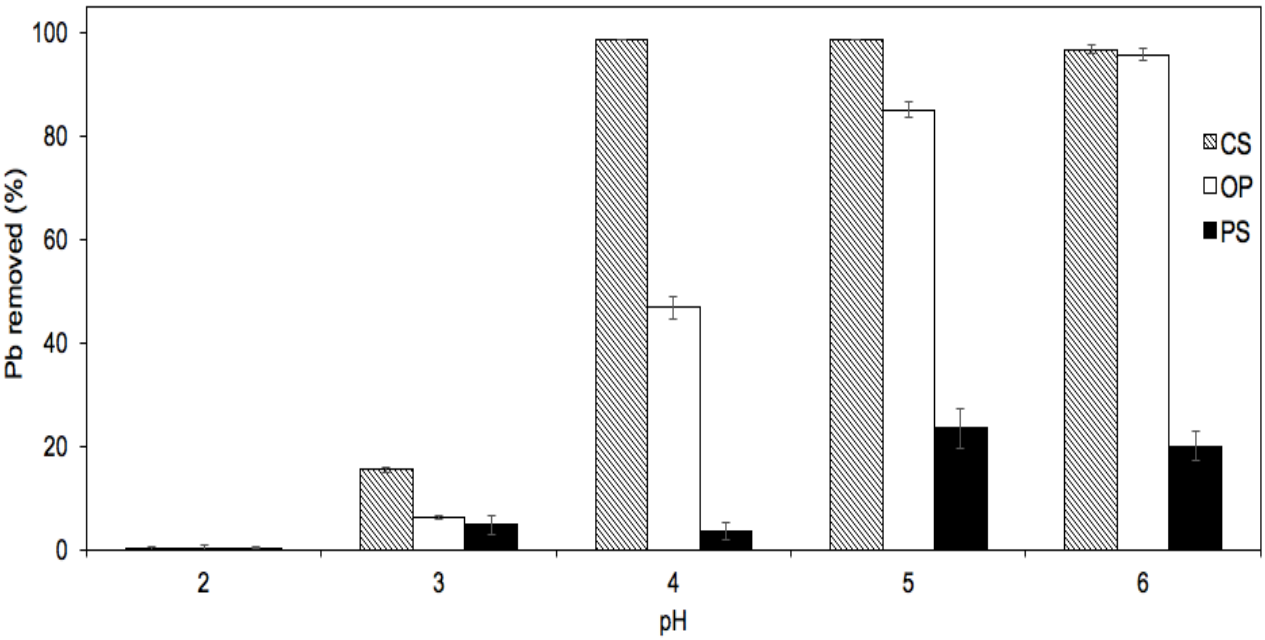

Figure 6. Adsorption of aqueous lead (Pb^{2+}) affected by solution pH (2-6): corn stover (CS), orange peel (OP), and pistachio shell (PS).

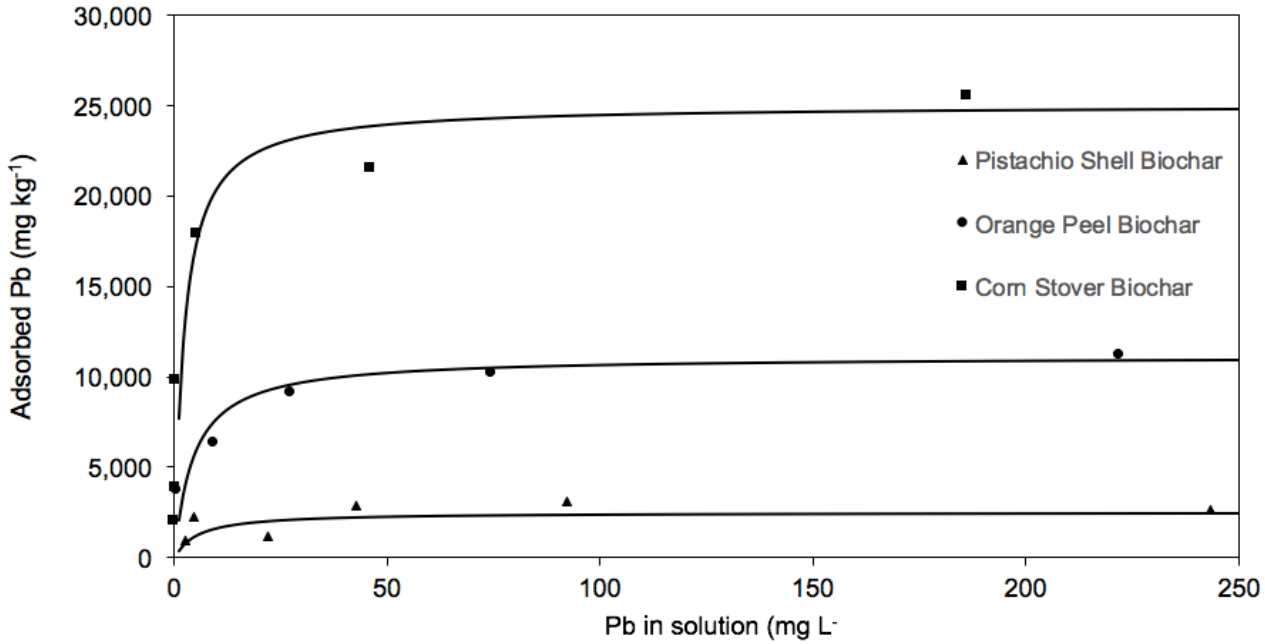

Figure 7. Lead adsorption isotherm affected by feedstock material. Solid lines indicate adsorption isotherm fitted with the Langmuir Model.

A

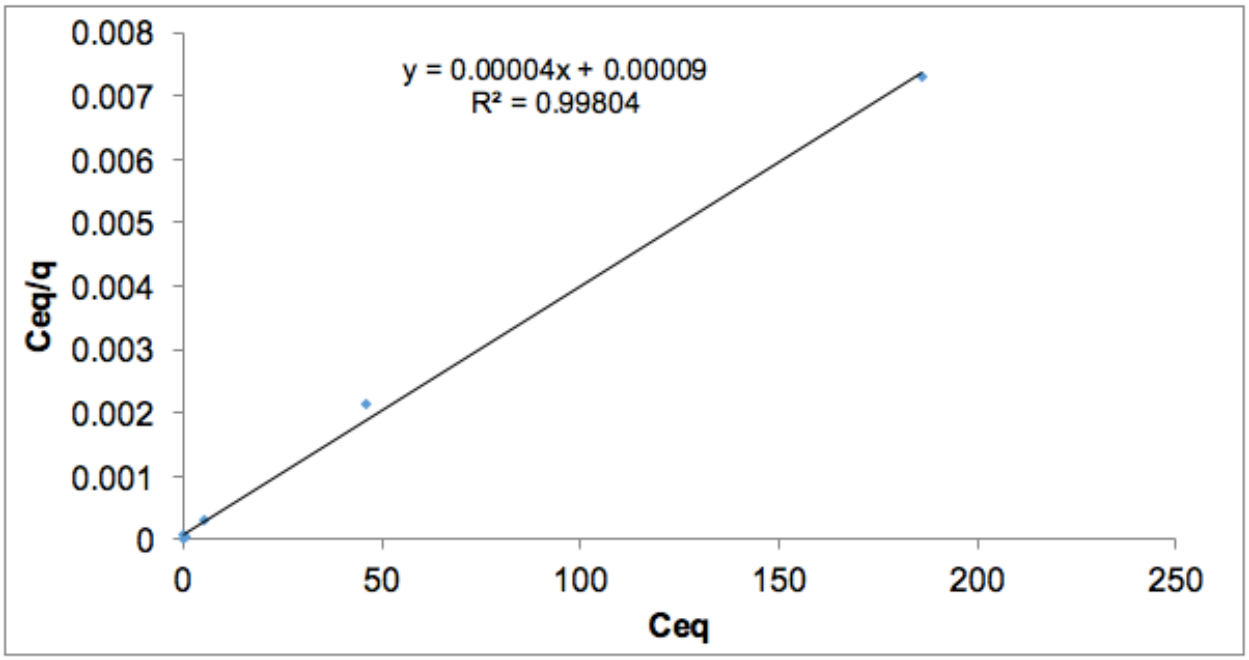

B

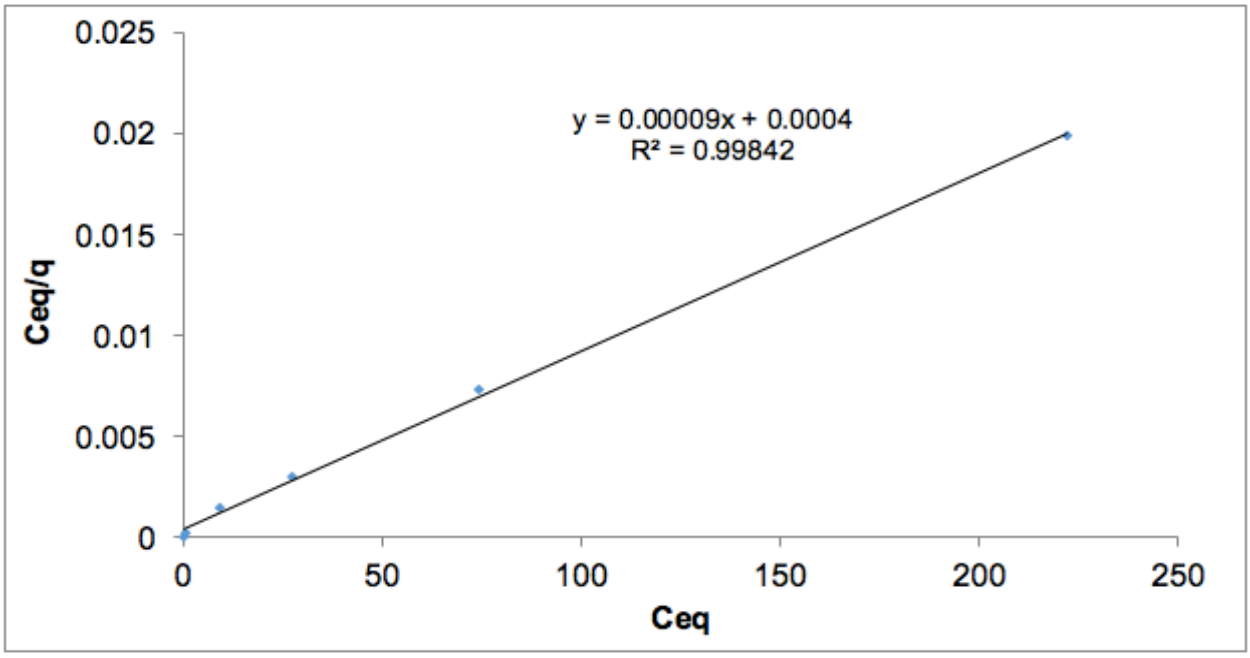

C

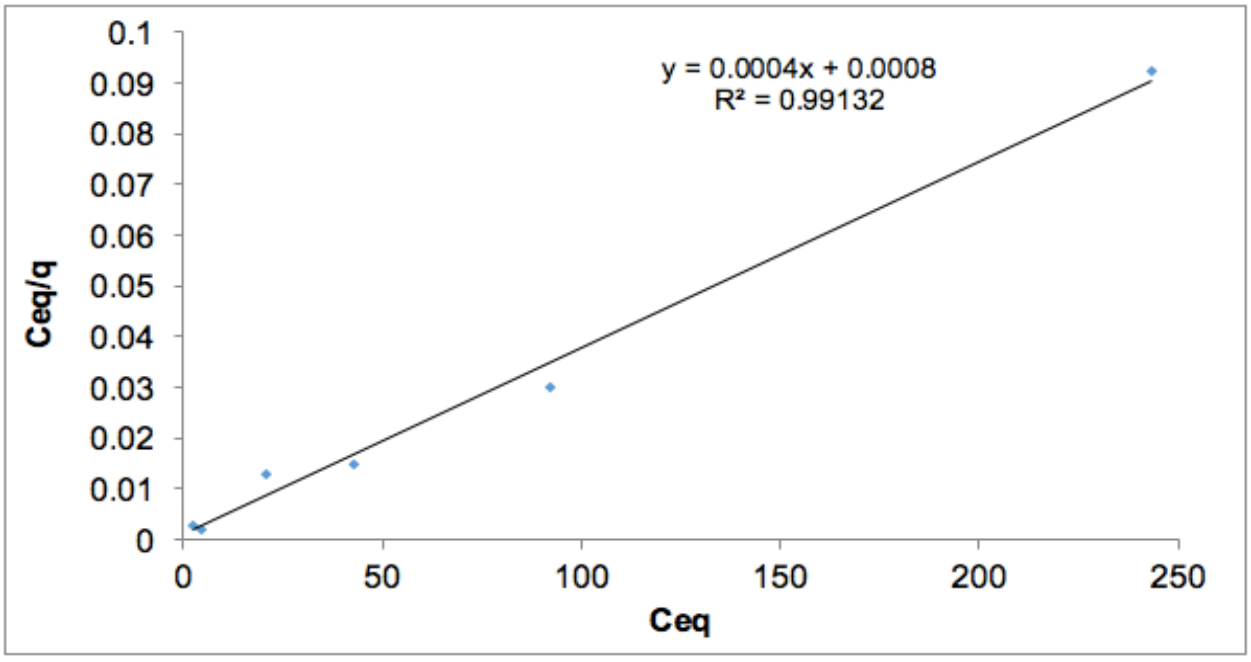

Figure 8. Langmuir isotherm plots for (A) CS600, (B) OP300, and (C) PS600

Table 1. Physiochemical properties of biochars produced by pyrolysis at 300, 450, and 600°C

Properties of char	*Types of Biochar*								
	CS300	CS450	CS600	OP300	OP450	OP600	PS300	PS450	PS600
Biochar Yield (%)	36.66	25.41	21.25	42.88	29.25	25.80	42.40	24.32	20.23
pH	8.16	8.38	8.72	8.99	9.34	9.37	7.36	7.49	7.52
EC ($\mu S\ cm^{-1}$)	284.00	327.00	457.00	278.00	606.00	725.00	151.30	165.30	181.90
SA(m^2/g^{-1})	1.432	1.071	3.623	8.873	0.811	2.208	0.980	3.323	268.94
Moisture (%)	1.00	2.00	2.00	1.60	2.50	1.00	1.00	2.60	2.60
Ash (%)	1.00	2.00	2.00	4.00	5.00	5.20	1.00	2.60	2.60
C (wt. %)	79.97	84.43	87.33	77.11	83.99	91.98	81.58	88.33	92.08
O (wt. %)	20.03	14.73	11.14	22.89	16.01	8.02	18.36	11.55	7.78
Na (wt. %)	-	-	-	-	-	-	0.06	0.11	0.19
Mg (wt. %)	-	-	-	-	-	-	-	-	-
Ca (wt. %)	-	-	-	-	-	-	-	-	-
O/C	0.18	0.13	0.09	0.22	0.14	0.06	0.16	0.09	0.06

Table 2. Parameters for the Langmuir and Freundlich adsorption model

Adsorption model	*Parameter*	*CS600*	*OP300*	*PS600*
Langmuir	Linearized equation	$y = 0.00004x + 0.00009$ ($R^2 = 0.99$)	$y = 0.00009x + 0.0004$ ($R^2 = 0.99$)	$y = 0.0004x + 0.0008$ ($R^2 = 0.99$)
	S_{max} (mg kg^{-1})	25,000	11,111	2,500
	K_L (L mg^{-1})	0.44	0.23	0.50
Freundlich	Linearized equation	$y = 0.2981x+3.79$ ($R^2 = 0.58$)	$y = 0.266x+3.49$ ($R^2 = 0.84$)	$y = 0.1749x+3.01$ ($R^2 = 0.43$)
	K_F (mg kg^{-1})	6,217	3,129	1024
	n (L kg^{-1})	3.35	3.75	5.72

CHAPTER III

ARSENIC (III) AND ARSENIC (V) REMOVAL USING MAGNETIC ORANGE PEEL BIOCHAR

3.1 Introduction

Arsenic (As) is a carcinogenic trace metal that poses a threat to human and ecosystem health. Serious human health risk imposed by As is attributed to As-contaminated drinking water as evidenced in the groundwater system in Bangladesh and India (Fendorf et al., 2010). As exists in several oxidative stages in nature, but inorganic forms of As (III) in in arsenite (AsO_3^{3-}) and As (V) in arsenate (AsO_4^{3-}) are the two main forms of arsenic found surface water and groundwater (Samsuri et al., 2013). As (III) has been found to be more toxic than As (V) because As (III) tends to inhibit the metabolic enzyme named pyruvate dehydrogenase, which is responsible for the conversion of pyruvate to acetyl CoA (Dong, 2014). The World Health Organization recommends maximum limit of 0.01 mg L^{-1} in drinking water (Tian et al., 2011).

Various techniques have been implemented to treat As-contaminated water including precipitation, ion exchange, membrane filtration, and oxidation (Mohan & Pittman, 2007). Adsorption technique has been an effective technique for treating As-contaminated water due to its cost-effectiveness, simple operation and less waste generation. Current research has focused on utilizing lost cost adsorbents and magnetic nanoparticles to remediate contaminated water (Baig et al., 2014;Kango & Kumar, 2016)

Biochar is carbon-rich porous material produced by the thermal conversion of biomass in an oxygen-free environment (pyrolysis). Biochar has been been shown to serve as a multifunctional material for enhancing soil fertility and remediating various organic and inorganic contaminants in water and soil environments (Wu et al., 2016). Due to its favorable physical and chemical properties such as microporous structure, O-containing functional groups, and cation exchange capacity, biochar is often regarded as a friendly environmental adsorbent for cationic heavy metals such as lead, cadmium, and zinc in aqueous solution (Mohan et al., 2007; Yang et al., 2015; Mireles et al., 2016). However, As adsorption onto biochars has been found to be low as the surfaces of biochars are mostly negatively-charged and As itself is an oxyanion-forming element (Beesley & Marmiroli, 2011)

Several surface modification methods have been investigated to modify biochar to enhance its sorption of oxyanions through surface complexation (Chen et al., 2011; Wang et al., 2015; Thines et al., 2017). While As are known to accumulate on Al oxides, Fe (hydr)oxides, and clay minerals such as kaoline, montmorillonite, and illite, Fe oxides tended to show strong adsorption to both As (III) and As (V) in soil and sediment solids (Fendorf, 2010). Thus, an option to increase As adsorption onto biochars is to magnetize biochar with Fe oxides such as magnetite. Utilizing magnetic adsorbents for treating contaminated water has been viewed an emerging remediation technique due to its ease in separating the adsorbent from solution by applying a magnetic field (Baig et al., 2014).

There are three common techniques (pyrolysis, co-precipitation, and calcination method) available to produce magnetic biochar and co-precipitation is considered to be a simplest techniue on the production of magnetic particles (Thines et al., 2017). The objective of this study was to produce magnetic orange peel (OP) biochar produced by the co-precipitation of

magnetite to remove As (III) and As (V). The As (III) and As (V) sorption behavior onto the magnetic biochar was studied by conducting isotherm and pH studies. Different characterization methods including XRD, FTIR, and SEM were used to study the adsorption mechanisms of As (III) and As (V) onto the magnetic biochar.

3.2 Materials and Methods

3.2.1 Synthesis of the Magnetic Biochar

The OP was obtained from a local grocery store located in McAllen, Texas. The OP was washed three times with tap water and cut into small pieces. The biomass was then oven dried at 105°C for 24 h and pulverized using a coffee grinder. The OP was stored dry until further use.

The OP was pyrolyzed under an oxygen-free environment in a tube furnace (Lindberg/Blue M^{TM} 1100°C Tube Furnaces, ThermoFisher Scientific, Waltham, MA, USA). The biomass was purged with nitrogen gas for 45 minutes in the reaction vessel prior to being heated in the tube furnace. It was pyrolyzed at 300°C and carried at that peak temperature for 1 h under 5 L min^{-1} of continuous nitrogen flow rate. After the 1 h, the tube furnace was turned off and cooled until the temperature reached 90°C under the nitrogen gas flow. The biochar was further ground and screened through 250 μm sieve. Magnetite (Fe_3O_4) impregnated biochar was synthesized by a co-precipitation method in which a solute precipitates out from a solution through a carrier that forces the solute to bind it together (Thines et al., 2017). In order to obtain Fe-modified biochar, 5.96 g of Iron chloride tetrahydrate ($FeCl_2{\cdot}4H_2O$) was mixed with 1 L of millipore DI water in a stirrer. One gram of OP biochar was added to the solution and stirred until a homogenous mixture was achieved. A 100 ml of a 1 M NaOH solution was added using a variable flow pump to the solution. Once the 100 ml were dispersed onto the solution, the

mixture was heated at 100°C in a hot plate stirrer for 1.5 h and then cooled. The magnetized biochar was vacuum filtered and washed using acetone to remove residues and then air-dried for further use.

3.2.2 Characterization of Magnetic Biochar

The magnetized biochar was characterized for magnetite using Brucker Model D8 X ray diffractometer (XRD). The XRD data was collected using a CuKα source of γ=1.5418 A$^{\circ}$, scan angle 2θ=6-80 and a scan rate of 0.1 degree per minute. The surface morphology of the OP biochar was examined using a scanning electron microscope (SEM) instrument (ZEISS EVO LS10 Scanning Electron Microscope) before and after magnetization. The samples were coated with an alloy of gold and palladium, mounted on metal stubs using a double stick tape. The metal coating of a gold/palladium was used to prevent buildup of high voltage charges on the magnetic biochar surface. The elemental composition of the magnetic biochar was determined using SEM instrumentation equipped with energy dispersive X-ray spectroscopy (EDS). The EDX system works by categorizing emitted x rays based on the characteristic energy given by the sample (Chandler & Roberson, 2009). Surface area of biochar samples was determined by the Brunauer Emmett Teller (BET) multilayer adsorption method using a Quantachrome Nova 2200e instrument.

Functional groups on the surface of the biochar before and after magnetization were examined by Attenuated Toral Reflectance Fourier transform infrared spectrophotometer (ATR-FTIR) (Perkin Elmer., Waltham, MA). Spectras were obtained at the 4000-650 cm^{-1} region. The resulting spectras were the average of 4 scans, which were used to characterize the functional groups based on their respective absorbance peaks.

3.3.3 Metal Adsorption Experiments

Effect of Solution pH. The binding of As (III) and As (V) to the magnetized biochar was performed in the pH range of 2 through 6. Briefly, a 250 ml of 10 ppm of As (III) and As (V) was prepared by diluting arsenic stock solutions (1000 ppm) made up of potassium arsenate dehydrate ($K_2AsHO_4 \cdot 2H_2O$) and arsenic trioxide (As_2O_3). Adsorption reactions were conducted in 5-ml polyethylene tubes containing 10 mg of the respective magnetic-biochar materials with 4 ml aliquot of 10 ppm As (III) and As (V) solution. The samples were shaken on a rotating shaker (Nutating Mixer, VWR International, Radnor, PA) for 1 h. Control samples containing 10 ppm of As (III) and As (V) solution without the magnetic biochar were included. All tests were done in triplicate. After 1-h equilibration, samples were centrifuged at 3,200 rpm for 5 min. The supernatant from each sample was collected and analyzed for remaining As (III) or As (V) using inductively coupled plasma optical emission spectrometry (ICP-OES).

Arsenic Adsorption Isotherm. Ten milligram of the magnetic biochar was weighted in triplicates and placed in 5-ml polyethylene tubes. Each polyethylene tube contained 4 mL of either As (III) or As (V) solution with the concentrations of 0, 5, 10, 25, 50, 70, and 100 mg L^{-1} with the pH of the solution adjusted to 4 for As (III) and 2 for As (V). The test tubes were equilibrated on a rotating shaker (Nutating Mixer, VWR International, Radnor, PA) for 1 h. After 1-h equilibration, samples were centrifuged at 3,200 rpm for 5 min. The supernatant from each sample were decanted and analyzed for remaining As using inductively coupled plasma optical emission spectrometry (ICP-OES).

The Langmuir and Freundlich isotherm models were used to study the adsorption mechanism of As (V) and As (III) to the magnetic biochar. The assumption of the Langmuir isotherm model is that molecules are adsorbed on definite sites on the surface of the adsorbent, and each site can accommodate only one molecule (monolayer) (Thirunavukkarasu et al., 2001; Zhang et al., 2013) The Freundlich isotherm model is based on multilayer adsorption which is often used to study the heterogeneous of the surface and the exponential distribution of sites and their energies (Tian et al., 2011). The two isotherm models can be expressed as Eqs (6) (7), respectively

$$q = (S_{max} K_L C)/(1 + K_L C) \quad (6)$$

$$q_e = K_F C_e^{1/n} \quad (7)$$

where

S_{max} is the maximum sorption capacity (mg kg^{-1}) and K_L is an affinity constant to bonding energy (L mg^{-1}). K_F and n are Freundlich constants measuring the adsorption capacity and adsorption intensity, C_e is the concentration of the adsorbate remaining in the solution, and q_e is the mass of the adsorbate per unit mass of adsorbent.

3.3 Results and Discussion

3.3.1 Magnetic Biochar Characterization

Figure 9 shows the powder XRD pattern of the magnetic biochar. Various sharp iron oxide peaks were observed in the 2θ range of 6-80° for the magnetic biochar. The Bragg peaks at 30.22, 35.55, 43.17. 53.6, 57.03, 62.83 in 2θ correspond to synthetic Fe_3O_4, according to the Powdered Diffraction File. The association of the Fe_3O_4 particles on the biochars surface was confirmed from the SEM micrograph, as shown in Fig 10. A good coating of the precipitated Fe_3O_4 on the magnetic biochars surface was achieved. Most of the magnetite particles appear to be an agglomeration of different particle sizes. Based on the SEM image, OP biochar served its main function as to providing a template material for Fe_3O_4 loading. Fig 11, presents the FTIR patterns for the magnetic biochar. Various bands in the FTIR spectra show different functional groups present on the surface of the Fe_3O_4/biochar. The peak at 3630 cm^{-1} represents the stretching and vibration of –OH (Peng et al., 2016). The band at 2931 cm^{-1} is attributed to asymmetric and symmetric C-H vibrations of the methylene groups. The characteristic band at 1560 cm^{-1} can be attributed to asymmetric and symmetric COO- stretches et (Wang et al., 2010). The band at 1060 cm^{-1} can be assigned to the bending vibration of hydroxyl group on metal oxides M-OH (Li et al., 2010).

3.3.2 Effect of Solution pH

The results in Fig 12 shows the effects of pH on As (III) and As (V) adsorption. The removal of As (V) was dependent on the pH of the solution with the greatest adsorption occurring during acidic conditions (pH 2) and decreased as the solution pH increased. The opposite trend was observed for As (III) removal, which was observed to be relatively constant from pH 4 to pH 6. Different arsenic ion species in solution have been known to exist based on the pH of the solution. As (V) tends to be present in solution as $H_2AsO_4^-$ at low pH values (< pH 6.9), which is negatively charged anion (Mohan and Pittman, 2007). The point zero charge (pzc) of the adsorbent played a critical role in the removal of arsenate. PZC refers to the certain pH at which the charge on the surface of an iron oxide is zero. Generally, the pzc of magnetite seems to be around pH 7.9(Cornell and Schwertmann, 2006) The surface of the iron oxides tends to become positively charged when the pH of the solution is below the pH_{PZC}, and negatively charged when the pH of the solution is above the pH_{PZC} (Wang et al., 2014). The removal of As (V) was more effective when the surface charge of the magnetic biochar was positively charged at an acidic pH. At an alkaline pH, the surface charge of the magnetite became negatively charged, and electrostatic repulsion starts to occur between the negatively charged H_2AsO^{4-} ion and the negatively charged surface of the magnetite (Pajany et al., 2011). From Fig 12, it can seen that the removal efficiency of As (V) decreases from 90% to 16% as the pH of the solution increased from pH 2 to pH 6. Moreover, trivalent forms of As tend to remain stable as non-ionic (H_3AsO_3) species in the pH range of 2.0-6.0, while anionic species ($H_2AsO_3^{-1}$ and $HAsO_3^{-2}$) species exist in the pH range of 7.5-9.0 (Vithanage et al., 2017; Kango and Kumar, 2016). As it is evident from Fig 10, the adsorption of As (III) over the pH range of 2-6 was not strongly dependent on the pH of the solution, which is an advantage for practical applications since no pH

adjustment has to be made. The removal efficiency of As (III) in the pH range of 4-6 was 57%, 56%, and 52%, respectively. The adsorption of As (III) could be explained by the interaction between the surface of the adsorbent and the adsorbate. In acidic conditions, the neutral H_3AsO_3 species comes in contact with the positively charged surface of the magnetic biochar which helps in the conversion of the non-ionic arsenic to its anionic form (Kundu and Gupta, 2006). Kangu and Kumar (2016), have stated that at pH values of 6.6 to 8.0, the neutral As (III) ions dissociate and produce anionic $H_2AsO_3^{-1}$ and $HAsO_3^{-2}$ which are attracted to the positively charged surface of the magnetite, enhancing As (III) removal. At higher pH values (pH>8), above the pH_{PZC} (7.9), the adsorbent surface becomes negatively charged, decreasing the removal of the anionic arsenic (III) species due to the repulsion forces between the negative surface of the magnetite and the anions.

3.3.3 Adsorption Isotherm

In this study, adsorption isotherms were performed at ambient temperature (25°C) and the pH adjusted at pH 2 for As (V) and pH 4 for As (III) according to the findings presented in the previous section.

The isotherms for the binding of As (III) and As (V) to the magnetic biochar were found to be fitted best with the Langmuir isotherm (Table 3) (Fig. 7). The corresponding correlation coefficient (R^2) for the fitting of the Langmuir isotherm were 0.97 for As (III) and 0.99 for As (V) but lower for the Freundlich model (R^2 = 0.89-0.93). Furthermore, the Langmuir isotherm model indicate that both As III) and As (V) bound to magnetic biochar with monolayer adsorption on a homogenous surface. This results are consistent with similar studies with the

reported mechanism of As (V) removal by monolayer adsorption onto maghemite nanoparticles (γ-Fe_2O_3) (Tuutijarvi et al., 2009).

The maximum adsorption capacity S_{max} (mg kg^{-1}) for As (III) adsorption was 9090.91mg kg^{-1} compared to 8333.33 mg kg^{-1} for As (V) (Table 3) (Fig. 13) (Fig. 14) The anionic arsenic species (e.g. H_2AsO^{4-}, H_3AsO) found within the pH range of 2-6 act as ligands, since they possess one or more atoms with a lone pair of electrons and so can function as the electron donor (Lewis Base) in a coordinate bond (Cornell and Schwertmann, 2006). Ligands absorb onto Fe oxides surface specifically by replacing the hydroxyl groups by the adsorbing ligand to form surface complexes. Generally, As (V) is more strongly adsorbed onto metal oxides given than As (III) is predominantly non-charged at pH values less than 9.2. This makes As (III) less available for precipitation, adsorption, or ion exchange (Nicomel et al., 2016)

3.4 Conclusion

The present study suggests that magnetic biochar is a promising and effective adsorptive material for the removal of As (III) and As (V) in solution. The adsorption of arsenic varies depending on different conditions. The optimal pH for the removal of As (V) was about 2, while the optimal pH for As (III) ranged from pH 4-6. SEM images showed that orange peel biochar served as a good template material for the precipitation of magnetite on its surface. The adsorption isotherms were well fitted using the Langmuir model. The adsorption capacity for As (III) and As (V) from the Langmuir isotherm were 9090.91mg $kg^{-}$and 8333.33 mg kg^{-1}, respectively. The arsenic removal mechanisms can be attributed to the electrostatic attraction between the hydroxyl functional groups and the As (III) and As (V) species. Hence, magnetic orange peel biochar showed that it has the potential in treating arsenic contaminated water.

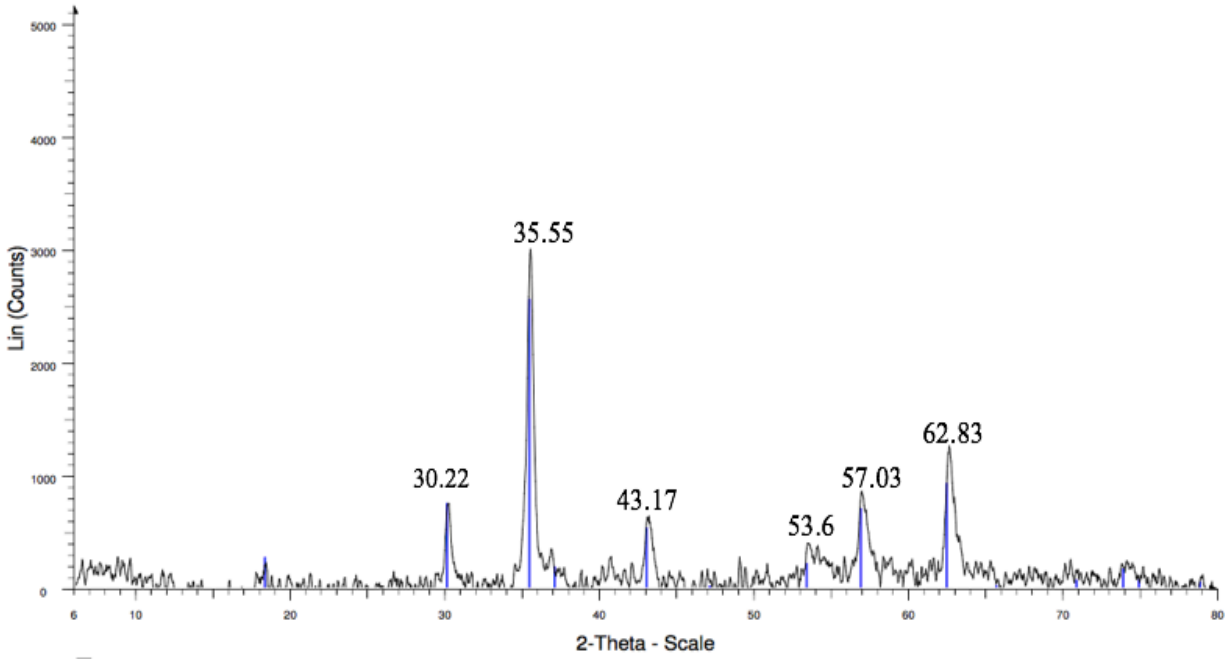

Figure 9: X-ray diffraction pattern of magnetic biochar

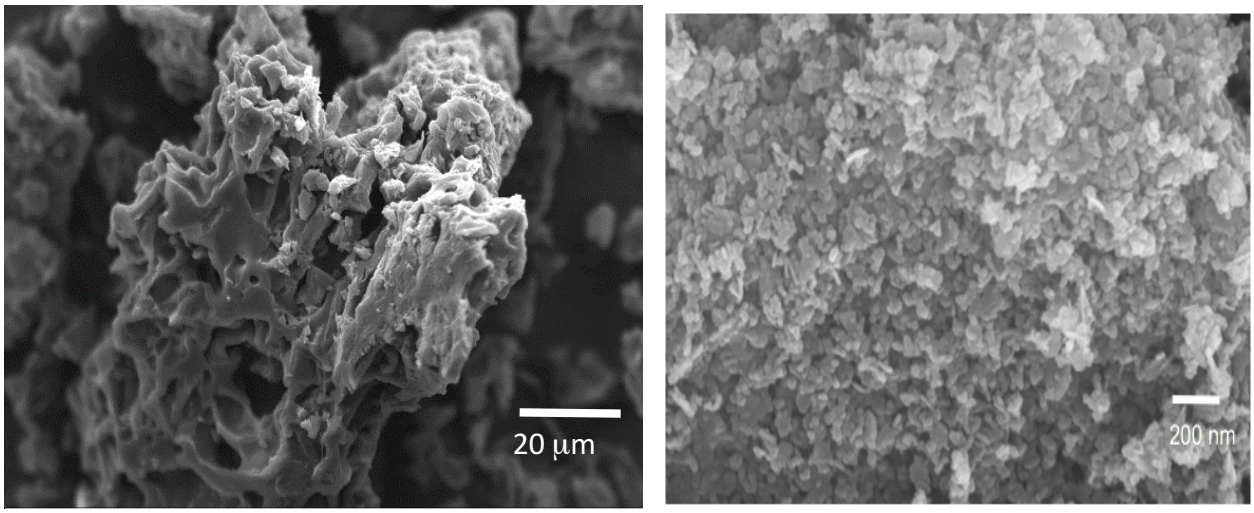

Figure 10. SEM images of unmagnetized and magnetized biochars

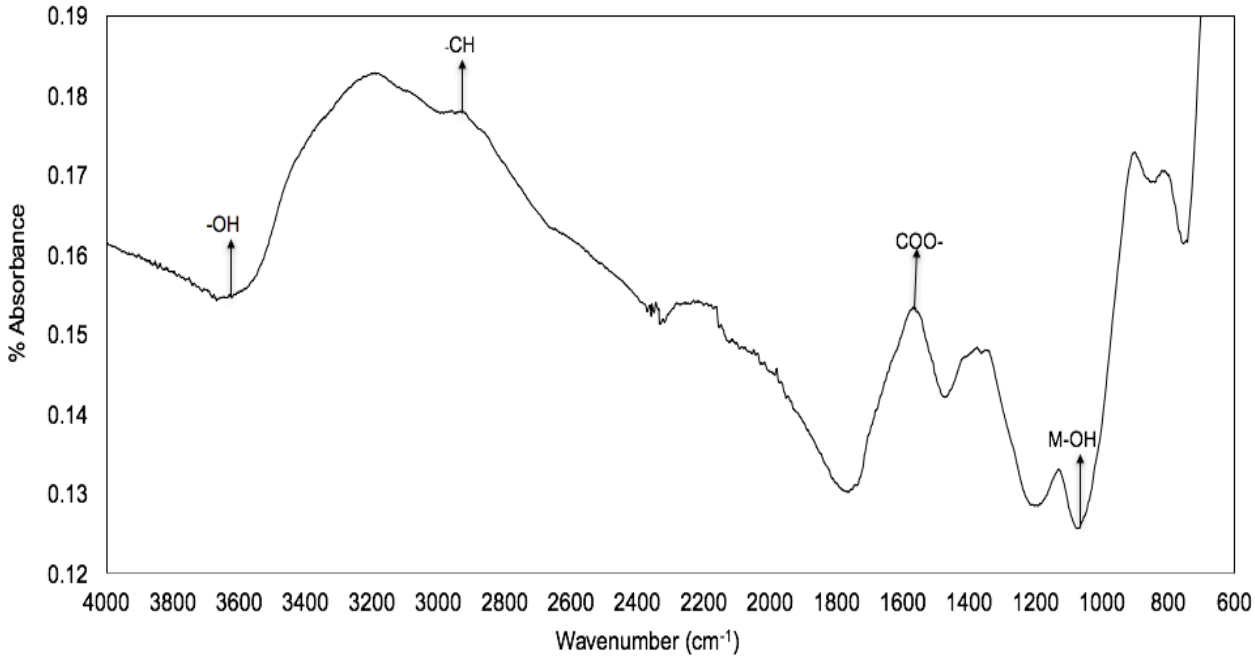

Figure 11: FTIR spectra of magnetic biochar

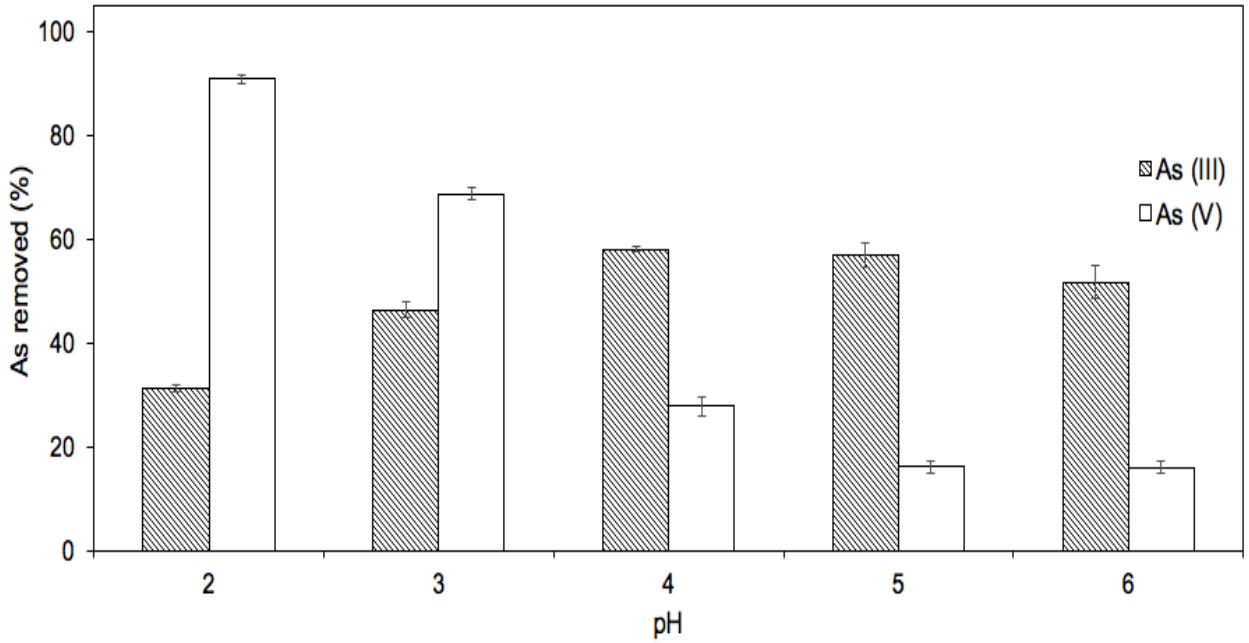

Figure 12: Adsorption of aqueous As (III) and As (V) onto magnetic biochar affected by solution pH (2-6)

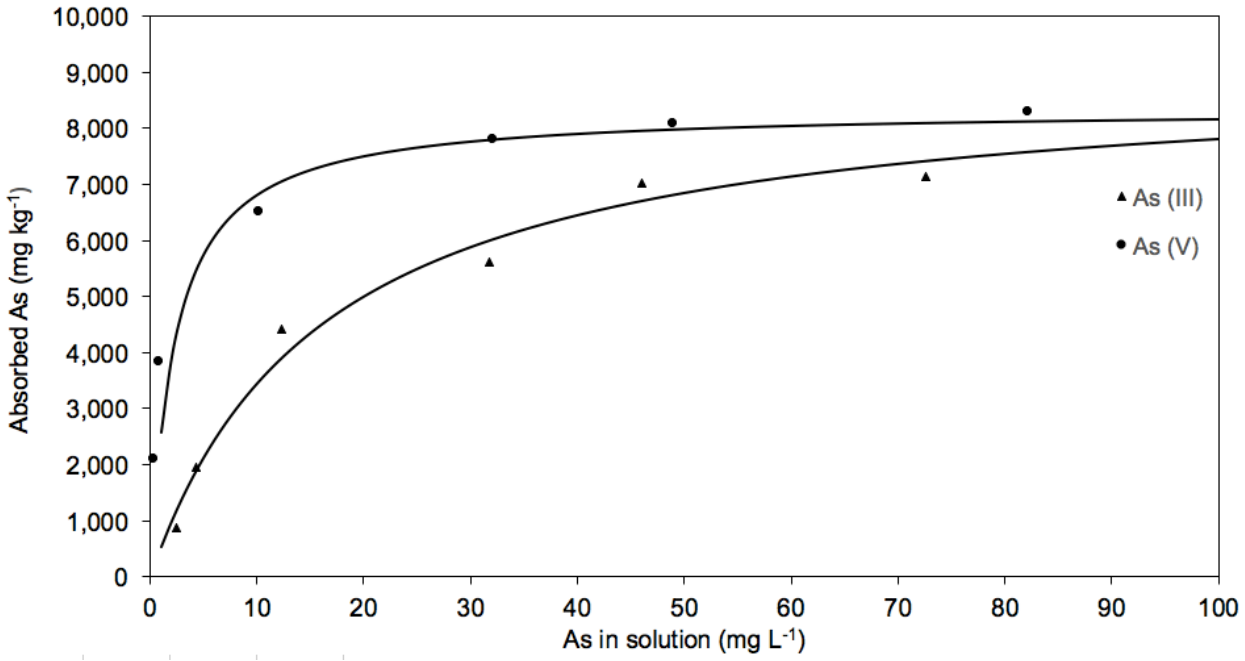

Figure 13. As (III) and As (V) adsorption isotherm onto magnetic biochar. Solid lines indicate adsorption isotherm fitted with the Langmuir Model.

A

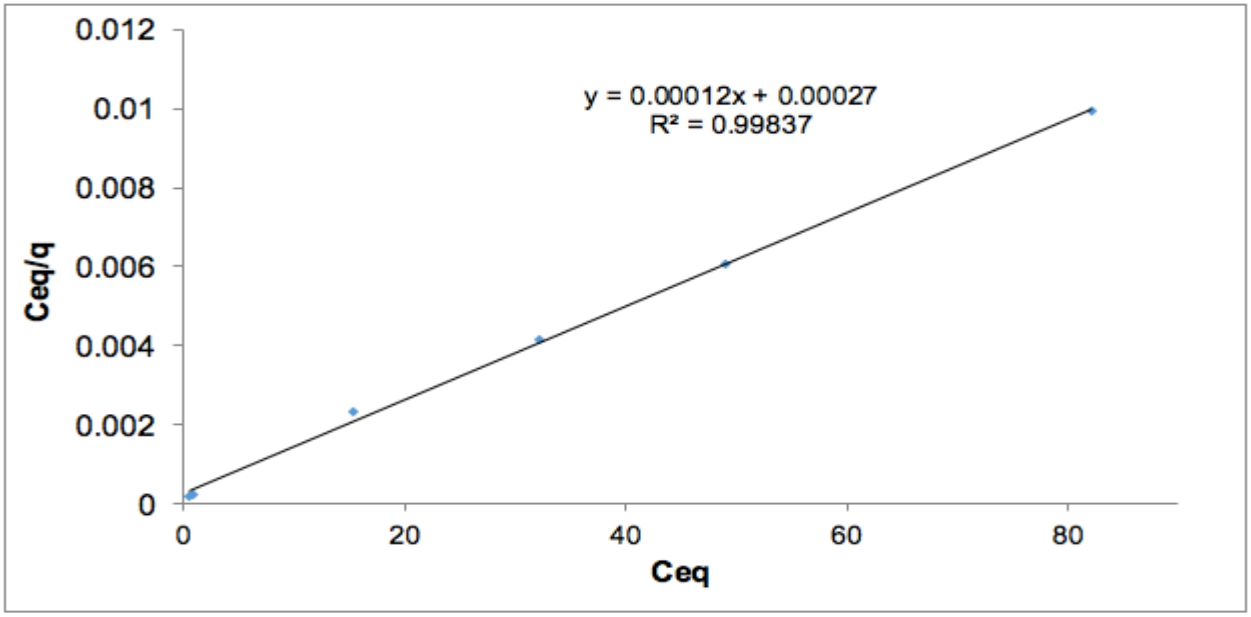

B

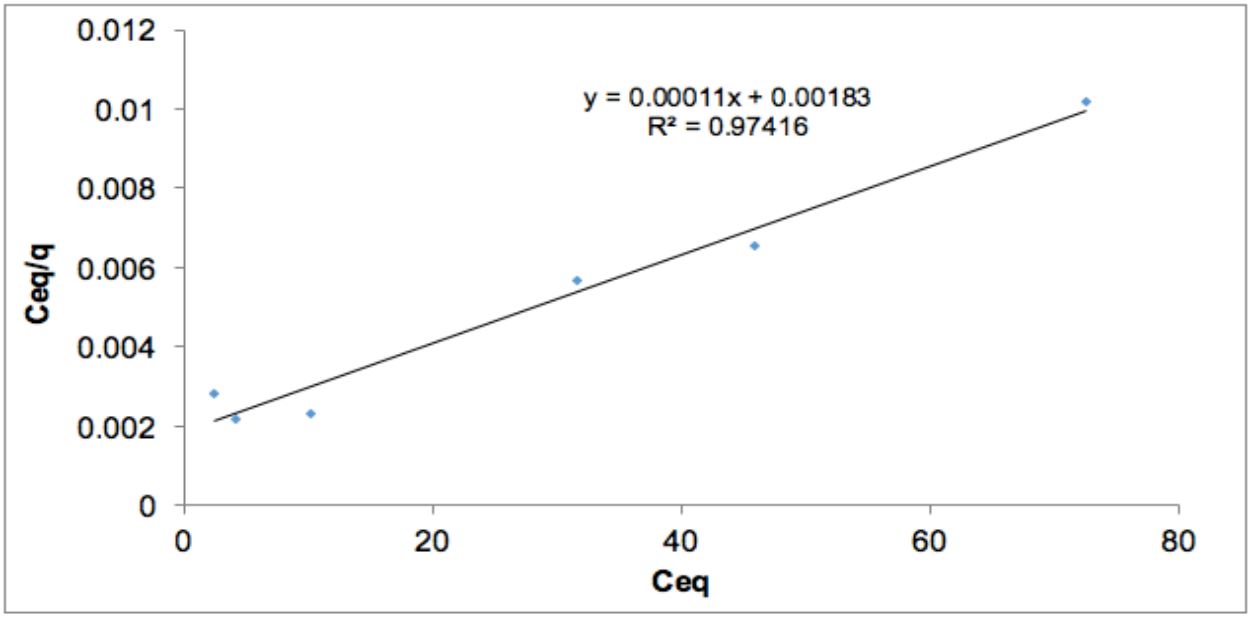

Figure 14. Langmuir isotherm plots: (A) As (III) and (B) As (V).

Table 3. Parameters for the Freundlich and Langmuir adsorption models for magnetic biochar.

Adsorption model	Parameter	As (III)	As (V)
Langmuir	Equation	y = 0.00011x + 0.00180 (R^2 = 0.97)	y = 0.00012x + 0.00027 (R^2 = 0.99)
	S_{max} (mg kg^{-1})	9090.91	8333.33
	K_L (L kg^{-1})	0.06	0.44
Freundlich	Equation	y = 0.5768x + 2.8746 (R^2 = 0.88)	y = 0.2433x + 3.4999 (R^2 = 0.93)
	K_F (mg kg^{-1})	741.31	3155.00
	n (L kg^{-1})	1.73	4.11

REFERENCES

Agrafioti, E., Kalderis, D., Diamadopoulos. "Arsenic and chromium removal from water using biochars derived from rise husk, organic solid wastes and sewage sludge." *Journal of Environmental Management* (2014): 309-314.

Ahmad, M., Rajapaksha, A., Lim, J., Zhang, M., Bolan, N., Mohan, D., Vithanage, M., Lee, S., Ok, Y. "Biochar as a sorbent for contaminant management in soil and water : A review." *Chemosphere* (2014): 19-33.

Al-Wabel, M., Al-Omran, A., El-Naggar, A., Nadeem, M. "Pyrolysis temperature induced changes in characteristics and chemical composition of biochar produced from conocarpus waste." *Bioresource Technology* (2013): 374-379.

Baig, S.A., Zhu, J., Muhammad, N., Sheng, T., Xu, X. "Effect of synthesis methods on magnetic Kans grass biochar for enhanced As (III, V) adsorption from aqueous solutions." *Biomass & Energy* (2014): 299-310.

Bailey, S., Olin, T., Bricka, R., Adrian, D. "A review of potentially low-cost sorbents for heavy metals." *Water Research* (1999): 2469-2479.

Baird, C. *Environmental Chemistry*. W.H. Freeman and Company, 2003.

Bandosz, Teresa J. *Activated Carbon Surfaces in Environmental Remediation*. Elsevier, 2006.

Bertocchi, A., Ghiani, M., Peretti, R., Zucca, A. "Red mud and fly ash for remediation of mines sites contaminated with As, Cd, Cu, Pb, and Zn." *Journal of Hazardous Materials* (2006): 112-119.

Beesley, L., & Marmiroli, M. (2011). The immobilisation and retention of soluble arsenic, cadmium and zinc by biochar. Environmental Pollution, 159(2), 474-480.

Cantrell, K.B., Hunt, P.G., Uchimiya, M., Novak, J.M., Ro, K. "Impact of pyrolysis temperature and manure source on physicochemical characteristics of biochar." *Bioresource Technology* (2012): 419-428.

Chandler, D., Roberson, R. *Bioimaging: Current concepts in light and electron microscopy*. Jones and Bartlett, 2009.

Chen, B., Chen, Z. "Sorption of Napthalene and 1-Naphthol by biochars of orange peels with different pyrolytic temperatures." *Chemosphere* (2009): 127-133

Chen, B., Chen, Z., & Lv, S. (2011). A novel magnetic biochar efficiently sorbs organic pollutants and phosphate. Bioresource technology, 102(2), 716-723.

Chen, X., Chen, G., Linggui, C., Yingxu, C., Lehmann, J., McBride, M., Hay, A. "Adsorption of copper and zinc by biochars produced from pyrolysis of hardwood and corn straw in aqueous solution." *Bioresource Technology* (2011): 8877-8884.

Cheng, W-H. "Torrefaction." *Pretreatment of Biomass: Processes and Technologies*. 2015.

Chowdhury, S., Mazumber, M., Al-Attas, O., Husain, T. "Heavy metals in drinking water: Occurrences, implications, and future needs in developing countries." *Science of the Total Environment* (2016): 569-570.

Chun, Y., Sheng, G., Chiou, C., Xing, B. "Compositions and sorptive properties of crop residue derived chars." *Environmental Science Technology* (2004): 4649-4655.

Cornell, R., Schwertmann, U. *The Iron Oxides: Structure, Properties, Reactions, Occurrences and Uses*. 2006.

Cui, X., Fang, S., Yao, Y., Li, T., Ni, Q., Yang, X., He, Z. "Potential mechanisms of cadmium removal from aqueous solution by Canna indica derived biochar." *Science of the Total Environment* (2016): 517-525.

Demirbas, A. "Heavy metal adsorption onto agro-based waste materials: ." *Journal of Hazardous Materials* (2008): 220-229.

Ding, W., Dong, X., Ime, I., Gao, B., Ma, L. "Pyrolytic temperature impact lead sorption mechanisms by bagasse biochars." *Chemosphere* (2014): 68-74.

Dong, M.H. *An Introduction to Environmental Toxicology* . n.d.

Erdem, E., Karapinar, N., Donat, R. "The removal of heavy metal cations by natural zeolites." *Journal of Colloid and Interface Science* (2004): 309-314.

Fendorf, S., Nico, P. S., Kocar, B. D., Masue, Y., & Tufano, K. J. (2010). Arsenic chemistry in soils and sediments. *Developments in soil science*, *34*, 357-378.

Galinato, S., Yoder, J., Granatstein. "The economic value of biochar in crop production and carbon sequestration." *Energy policy* (2011): 6344-6350.

Gupta, V.K., Rastogi, A. "Biosorption of lead (II) from aqueous solutions by non-living algal biomass Oedogonium sp. and Nostoc sp.- A comparative study." *Colloids and Surfaces B: Biointerfaces* (2008): 170-178.

Herawati, N., Suzuki, S., Hayashi , K., Rivai, F., Koyama, H. "Cadmium, Copper, and Zinc Levels in Rice and Soil of Japan, Indonesia, and China by Soil Type." *Bulletin of Environmental Contamination and Toxicology* (2000): 33-339.

Higashikawa, F.S., Conz, R.F., Colzato, M., Cerri, C., Alleoni, L. "Effects of feedstock type and slow pyrolysis temperature in the production of biochars on the removal of cadmium and nickel from water." *Journal of Cleaner Production* (2016): 965-972.

Hoffman, D., Rattner, B., Burton, A., Cairns, J. *Handbook of Ecotoxicology*. Lewis Publishers , 2003.

Inyang, M., Gao, B., Yao, Y., Xue, Y., Zimmerman, A. R., Pullammanappallil, P., & Cao, X. "Removal of heavy metals from aqueous solution by biochars derived from anaerobically digested biomass." *Bioresource Technology* (2012): 50-56.

Jarup, L. "Hazards of heavy metal contamination." *British Medical Bulletin* (2003): 167-182.

Jin, J., Li, Y., Zhang, J., Wu, S., Cao, Y., Liang, P., Zhang, J., Wong, M., Wang, M., Shan, S., Christie, P. "Influence of pyrolysis temperature on properties and environmental safety of heavy metals in biochars derived from municipal sewage sludge." *Journal of Hazardous Materials* (2016): 417-426.

Jindo, K., Mizumoto, H., Sawada, Y., Monedero, A., Sonoki, T. "Physical and chemical characterization of biochars obtained from the fast pyrolysis of pitch pine." *Bioresource Technology* (2014): 6613-6621.

Kango, S., Kumar, R. "Low cost magnetic adsorbent for As (III) removal from water: adsorption kinetics and isotherms." *Environmental Monitoring and Assessment* (2016): 1-14.

Keiluweit, M., Nico, P. S., Johnson, M. G., & Kleber, M. (2010). Dynamic molecular structure of plant biomass-derived black carbon (biochar). *Environmental science & technology, 44*(4), 1247-1253.

Kim, KH., Kim, JY., Cho, TS., Choi, JW. "Influence of pyrolysis temperature on physicohemical properties of biochar obtained from the fast pyrolysis of pitch pine." *Bioresource Technology* (2012): 158-162.

Kobya, M., Dermirbas, E., Senturk, E., Ince, M. "Adsorption of heavy metal ions from aqueous solutions by activated carbon prepared from apricot stone." *Bioresource Technology* (2005): 1518-1521.

Komnitsas, K., Zaharaki, D., Pyliotis, I., Vamvuka, D., Bartzas, G. "Assessment of pistachio shell biochar quality and its potential for adsorption of heavy metals." *Waste and Biomass Valorization* (2015): 805-816

Kumar, S., Loganathan, V., Gupta, R., Barnett, M. "An assessment of U(VI) removal from groundwater using biochar produced from hydrothermal carbonization." *Journal of Environmental Management* (2011): 2504-2512.

Kundu, S., Gupta, A.K. "Adsorptive removal of As (III) from aqueous solution using iron oxide coated cement (IOCC): Evaluation of kinetic, equilibrium and thermodynamic models." *Separation and Purification Technology* (2006): 165-172.

Lakherwal, D. "Adsorption of Heavy Metals: A Review." *International Journal of Environmental Research and Development* (2014): 41-48.

Lehmann, J. "A handful of carbon." *Nature* (2007): 143-144.

Lehmann, J., Gaunt, J., Rondon, M. "Bio-char sequestration in terrestrial ecosystem-A review." *Mitigation and Adaptation Strategies for Global Change* (2006): 403-427.

Li, F., Shen, K., Long, X., W, J., Xie, X., Zeng, X., Liang, Y., Wei, Y., Lin, Z., Huang, W., Zhong, R. "Preparation and Characterization of Biochars from Eichornia crassipes for Cadmium Removal in Aqueous Solutions." *PLos ONE* (2016): 1-13.

Li, Z., Deng, S., Yu, G., Huang, J., Lim, V. "As (V) and As (III) removal from water by a Ce-Ti oxide adsorbent: Behavior and mechanism." *Chemical Engineering Journal* (2010): 106-113.

Liu, Z., Zhang, F. "Removal of lead from water using biochars prepared from hydrothermal liquefaction of biomass." *Journal of Hazardous Materials* (2009): 933-939.

Lo, W., Chua, H., Lam, K., and Bi, S. 1999. “A Comparative Investigation on the Biosorption of Lead by Filamentous Fungal Biomass”. Chemosphere. 39: 2723-2736.

Lorenzen, L., van Deventer, J.S.J., Landi, W.M. "Factors affecting the mechanism of the adsorption of arsenic species on activated carbon." *Minerals Engineering* (1995): 557-569.

Lu, H., Zhang, W., Yang, Y., Huang, X., Qiu, R. "Relative distribution of Pb sorption mechanisms by sludge-derived biochar." *Water Research* (2012): 854-862.

Lyu, H., Gong, Y., Gurav, R., Tang, J. "Potential Application of Biochar for Bioremediation of Contaminated Systems ." *Biochar Application* (2016): 221-246.

Mary, G., Sugumaran, P., Niveditha, S., Ramalakshmi., Ravachandran, P., Seshadri, S. "Production, characterization and evaluation of biochar from pod (Pisum sativum), leaf (Brassica oleracea) and peel (Citrus sinensis) wastes." *International Journal of Recycling of Organic Waste in Agriculture* (2016): 43-53.

Mireles, S., Ok, Y., Cheng, C., Kang, J. "Adsorptive and kinetic characterization of aqueous zinc removal by biochars." *Journal of Earth Sciences & Environmental Studies* (2016): 1-7.

Mohan, D., Pittman, C. "Arsenic removal from water/wastewater using adsorbents-A critical review." *Journal of Hazardous Materials* (2007): 1-53.

Mohan, D., Rajput, S., Singh, V., Steele, P., Pittman, C. "Modeling and evaluation of chromium remediation from water using low cost bio-char, a green adsorbent." *Journal of Hazardous Materials* (2011): 319-333.

Mukherjee, A., Bhattacharya, P. "Arsenic in groundwater in the Bengal Delta Plain: slow poisoning Bangladesh." *Environmental Reviews* (2001): 189-220.

Mukome, F. N., & Parikh, S. J. (2015). Chemical, Physical, and Surface characterization of Biochar. In Y.S. Ok (Ed.), Biochar: Production, Characterization, and Applications, (pp 68-96). Boca Raton, FL: CRC Press.

Nagajyoti, P.C., Lee, K.D., Sreekanth, T.V. "Heavy metals, occurrence and toxity for plants: a review." *Environmental Chemistry Letters* (2010): 199-216.

Nicomel, N.R., Leus, K., Folens, K., Van Der Voort, P., Laing, G. "Technologies for Arsenic Removal from Water: Current Status and Future Perspectives." *Journal of Environmental Research and Public Health* (2016): 1-24.

Pajany, Y., Hurel, C., Marmier, N., Romeo, M. "Arsenic (V) adsorption from aqueous solution onto goethite, hematite, magnetite, and zero-valent iron: Effects of pH, concentration and reversibility ." *Desalination* (2011): 93-99.

Peng, B., Song, T., Wang, T., Chai, L., Yang, W., Li, X., Li, C., Wang, H. "Facile synthesis of Fe3O4@Cu(OH)2 composites and their arsenic adsorption application." *Chemical Engineering Journal* (2016): 15-22.

Rehrah, D., Reddy, M., Novak, M.R., Bansode, R.R., Schimmel, K.A., Yu, J., Watts, D.W. "Production and characterization of biochars from agricultural by-products for use in soil quality enhancement." *Journal of Analytical and Applied Pyrolysis* (2014): 301-309.

Saeed, A., Akhter, M., Iqbal, M. "Removal and recovery of heavy metals from aqueous solutions using papaya wood as a new biosorbent." *Separation and Purification Technology* (2005): 25-31.

Samsuri, A.W., Zadeh, F.S., Seh-Bardan, B.J. "Adsorption of As (III) and As (V) by Fe coated biochars and biochars produced from empty fruit bunch and rice husk." *Journal of Environmental Chemical Engineering* (2013): 981-988

Shackley, S., Sohi, S., Ibarrola, R., Hammond, J., Masek, O., Brownsort, P., Cross, A., Prendergast, M., Haszeldine, S. "Biochar, Tool for Climate Change Mitigation and Soil Management." (2013): 73-140.

Smedley, P.L., Kinniburgh, D.G. "A review of the source, behavior, and distribution of arsenic in natural water." *Applied Geochemistry* (2002): 517-568.

Subbaiah, M. *Adsorption process in water treatment -Removal of metal ions*. Lambert Academic Publishing , 2011.

Sublet, R., Simonnot, M.O., Boireau, A., Sardin, M. "Selection of an adsorbent for lead removal from drinking water by a point use treatment device." *Water Research* (2003): 4904-4912.

Tan, C., Yaxin, Z., Hongtao, W., Wenjing, Lu., Zeyu, Z., Yuancheng, Z., Lulu, R. "Influence of pyrolysis temperature on characteristics and heavy metal adsorptive performance of biochar derived from municipal sewage sludge." *Bioresource Technology* (2014): 47-54.

Tan., X., Liu, Y., Zeng, G., Wang, X., Xinjiang, H., Yanling, G., Yang, Z. "Application of biochar for the removal of pollutants from aqueous solutions." *Chemosphere* (2015): 70-85.

Thines, K. R., Abdullah, E. C., Mubarak, N. M., & Ruthiraan, M. (2017). Synthesis of magnetic biochar from agricultural waste biomass to enhancing route for waste water and polymer application: A review. *Renewable and Sustainable Energy Reviews*, *67*, 2 57-276.

Thirunavukkarasu, O.S., Viraraghavan, T., Subramanian, K.S. "Removal of arsenic in drinking water by iron oxide-coated sand and ferrihydrite-batch studies." *Water Quality Research* (2001): 55-70.

Tian, Y., Wu, M., Lin, X., Huang, P., Huang, Y. "Synthesis of magnetic wheat straw for arsenic adsorption." *Journal of Hazardous Materials* (2011): 10-16.

Tuutijarvi, T., Lu, J., Sillanpaa, M., Chen, G. "As (V) adsorption on maghemite nanoparticles ." *Journal of Hazardous Materials* (2009): 1415-1420.

Uchimiya, M., Wartelle, L., Klasson, K., Fortier, C., Lima, I. "Influence of pyrolysis temperature on biochar property and function as a heavy metal sorbent in soil." *Journal of Agriculture and Food Chemistry* (2011): 2501-2510.

Van der Perk, M. (2013). Soil and water contamination. CRC Press.

Vithanage, M., Herath, I., Joseph, S., Bundschuh, J., Bolan, N., Ok, Y., Kirkham, M.B., Rinklebe, J. "Interaction of arsenic with biochar in soil and water: A critical review." *Carbon* (2017): 219-230.

Wang, C., Hong, J., Chen, G., Zhang, Y., Gu, N. "Facile method to synthesize oleic acid-capped magnetite nanoparticles ." *Chinese Chemical Letters* (2010): 179-182.

Wang, C., Luo, H., Zhang, Z., Wu, Y., Zhang, J., Chen, S. "Removal of As (III) and As (V) from aqueous solutions using nanoscale zero valent iron-reduced graphite oxide modified composites." *Journal of Hazardous Materials* (2014): 124-131.

Webb, P. "Introduction to Chemical Adsorption Analytical Techniques and their Applications to Catalysis." *Micromeritics Instrument Corp. Technical Publications* (2003).

Winsley, P. "Biochar and bioenergy production for climate change mitigation." *New Zealand Science Review* (2007): 5-10.

Worch, E. *Adsorption Technology In Water Treatment*. 2012.

Wu, W., Li, J., Niazi, N.K., Muller, K., Chu, Y., Zhang, L., Yuan, G., Lu, K., Song, Z., Wang, H. "Influence of pyrolysis temperature on lead immobilization by chemically modified coconut fiber-derived biochars in aqueous environments ." *Environmental Science and Pollution Research* (2016): 22890–22896.

Xu, D., Zhao, Y., Sun, K., Gao,B., Wang, Z., Wang, Z., Jin, J., Zhang, Z., Wang, S., Yan, Y., Liu, X., Wu, F. "Cadmium adsorption on plant-and manure derived biochars and biochar-amended sandy soils: Impacts of bulk and surface properties." *Chemosphere* (2014): 320-326.

Yang, H., Yann, R., Chen, H., Ho Lee, D., Zheng, C. "Characteristics of hemicellulose, cellulose, and lignin pyrolysis." *Fuel* (2007): 1781-1788.

Yang, X., Lu, K., McGrouther, K., Che, L., Hu, G., Wang, Q., Liu, X., Shen, L., Huang, H., Ye, Z., Wang, H. "Bioavailability of Cd and Zn in soils treated with biochars derived from tobacco stalk and dead pigs." *Journal of soils and sediments* (2015): 751-762.

Yap, M., Mubarak, N., Sahu, J., Abdullah. "Microwave induced synthesis of magnetic biochar from agricultural biomass for removal of lead and cadmium from wastewater." *Journal of Industrial and Engineering Chemistry* (2017): 287-295.

Yuan, JH., Xu, RK., Zhang, H. "The form of alkalis in the biochar produced from crop residues at different temperatures." *Bioresource Technology* (2011): 3488-3487.

Zama, E., Guan Zhu, Y., Reid, B., Xin Sun, G. "The role of biochar properties in influencing the sorption and desorption of Pb (II), Cd (II), and As (III) in aqueous solution." *Journal of Cleaner Production* (2017): 127-136.

Zhang, M., Gao, B., Varnoosfaderani, S., Hebard, A., Yao, Y., Inyang, M. "Preparation and characterization of a novel magnetic biochar for arsenic removal." *Bioresource Technology* (2013): 457-462.

Zhou, N., Chen, H., Xi, J., Yao, D., Zhou, Z., Tian, Y., Lu, X. "Biochars with excellent Pb (II) adsorption property produced from fresh and dehydrated banana peels via hydrothermal carbonization." *Bioresource Technology* (2017): 204-210.

APPENDIX A

Lead Single Point Adsorptions

Orange Peel	Sample	Controls	Average Control	Difference	% Bound	Aver % Bound
T= 300	0.605	9.639	9.5315	8.9265	93.6526255	94.2541398
	0.244	9.424		9.2875	97.4400671	
	0.794			8.7375	91.6697267	
T=450						
	2.444	9.639	9.5315	7.0875	74.3587053	74.2537901
	2.635	9.424		6.8965	72.3548235	
	2.283			7.2485	76.0478414	
T=600	1.991	9.639	9.5315	7.5405	79.1113676	75.8310165
	1.874	9.424		7.6575	80.3388764	
	3.046			6.4855	68.0428054	
Pistachio Shells						
T=300	7.548	9.639	9.5315	1.9835	20.809946	19.7503016
	7.543	9.424		1.9885	20.8624036	
	7.755			1.7765	18.6381997	
T=450						
	7.271	9.639	9.5315	2.2605	23.7160992	20.5336691
	7.616	9.424		1.9155	20.0965221	
	7.836			1.6955	17.7883859	
T=600	5.924	9.639	9.5315	3.6075	37.8481876	34.6552659
	6.582	9.424		2.9495	30.9447621	
	6.179			3.3525	35.1728479	
Corn Stover						
T= 300	2.055	8.97	9.027333333	6.97233333	77.2358024	68.5842995
	3.294	9.025		5.73333333	63.510819	
	3.159	9.087		5.86833333	65.0062772	
T=450						
	1.203	8.97	9.027333333	7.82433333	86.6738055	89.3619378
	1.039	9.025		7.98833333	88.4905103	
	0.639	9.087		8.38833333	92.9214977	
T=600	0.0613	8.97	9.027333333	8.96603333	99.3209512	98.2228048
	0.198	9.025		8.82933333	97.8066613	
	0.222	9.087		8.80533333	97.540802	

Effect of solution pH: (A) Corn Stover (B) Orange Peel (C) Pistachio Shells

A

Controls	Concentration	Average C.	Samples	Concentration	mg/L bound	% bound	Ave. % bound
pH 2 C	9.300	9.333	pH 2 S	9.268	0.0653	0.70000	0.135714
pH 2 C	9.400		pH 2 S	9.405	-0.0717	-0.76786	
pH 2 C	9.300		pH 2 S	9.289	0.0443	0.47500	
pH 3 C	8.622	8.704	pH 3 S	7.275	1.4290	16.41774	15.494792
pH 3 C	8.584		pH 3 S	7.355	1.3490	15.49862	
pH 3 C	8.906		pH 3 S	7.436	1.2680	14.56801	
pH 4 C	8.229	8.104	pH 4 S	0.122	7.9823	98.49463	98.457615
pH 4 C	8.106		pH 4 S	0.125	7.9793	98.45762	
pH 4 C	7.978		pH 4 S	0.128	7.9763	98.42060	
pH 5 C	8.186	8.170	pH 5 S	0.113	8.0573	98.61695	98.490474
pH 5 C	8.247		pH 5 S	0.122	8.0483	98.50679	
pH 5 C	8.078		pH 5 S	0.135	8.0353	98.34768	
pH 6 C	7.191	7.526	pH 6 S	0.177	7.3493	97.64826	96.634040
pH 6 C	7.838		pH 6 S	0.212	7.3143	97.18322	
pH 6 C	7.550		pH 6 S	0.371	7.1553	95.07064	

B

Controls	Concentration	Average C.	Samples	Concentration	mg/L bound	% bound	Ave. % bound
pH 2 C	9.660	9.633	pH 2 S	9.657	-0.0243	-0.25261	0.020763
pH 2 C	9.750		pH 2 S	9.748	-0.1153	-1.19731	
pH 2 C	9.488		pH 2 S	9.487	0.1457	1.51222	
pH 3 C	8.591	8.626	pH 3 S	8.160	0.4657	5.39862	6.225606
pH 3 C	8.607		pH 3 S	8.041	0.5847	6.77822	
pH 3 C	8.679		pH 3 S	8.065	0.5607	6.49998	
pH 4 C	7.855	7.670	pH 4 S	3.909	3.7610	49.03520	46.718818
pH 4 C	7.481		pH 4 S	4.422	3.2480	42.34681	
pH 4 C	7.674		pH 4 S	3.929	3.7410	48.77445	
pH 5 C	8.220	7.933	pH 5 S	1.087	6.8463	86.29832	84.949580
pH 5 C	7.862		pH 5 S	1.417	6.5163	82.13866	
pH 5 C	7.718		pH 5 S	1.078	6.8553	86.41176	
pH 6 C	7.602	7.593	pH 6 S	0.493	7.0997	93.50689	95.622970
pH 6 C	7.234		pH 6 S	0.250	7.3427	96.70735	
pH 6 C	7.942		pH 6 S	0.254	7.3387	96.65467	

C

Controls	Concentration	Average C.	Samples	Concentration	mg/L bound	% bound	Ave. % bound
pH 2 C	9.577	9.604	pH 2 S	9.547	0.0567	0.59005	0.364444
pH 2 C	9.638		pH 2 S	9.604	-0.0003	-0.00347	
pH 2 C	9.596		pH 2 S	9.555	0.0487	0.50675	
pH 3 C	8.813	8.965	pH 3 S	8.720	0.2447	2.72923	4.711088
pH 3 C	8.999		pH 3 S	8.700	0.2647	2.95233	
pH 3 C	9.082		pH 3 S	8.207	0.7577	8.45170	
pH 4 C	7.888	7.838	pH 4 S	7.764	0.0740	0.94412	3.466020
pH 4 C	7.950		pH 4 S	7.609	0.2290	2.92166	
pH 4 C	7.676		pH 4 S	7.326	0.5120	6.53228	
pH 5 C	7.567	7.719	pH 5 S	6.222	1.4970	19.39370	23.439997
pH 5 C	7.690		pH 5 S	5.326	2.3930	31.00143	
pH 5 C	7.900		pH 5 S	6.181	1.5380	19.92486	
pH 6 C	7.230	7.158	pH 6 S	6.082	1.0760	15.03213	19.870541
pH 6 C	7.171		pH 6 S	5.378	1.7800	24.86728	
pH 6 C	7.073		pH 6 S	5.747	1.4110	19.71221	

Adsorption isotherms: (A) Corn Stover (B) Orange Peel (C) Pistachio Shells

A

Controls	Concentration	Average	Sample	Concentration	mg/L Bound	%Bound	Percent Bound
5 ppm	4.97	4.93	5 ppm	0.000	4.97	100.00	100.00
5 ppm	4.88		5 ppm	0.000	4.88	100.00	
5 ppm	4.93		5 ppm	0.000	4.93	100.00	
10 ppm	9.72	9.71	10 ppm	0.32	9.40	96.71	96.77
10 ppm	9.78		10 ppm	0.29	9.49	97.03	
10 ppm	9.62		10 ppm	0.33	9.29	96.57	
25ppm	24.83	24.78	25ppm	0.439	24.39	98.23	98.42
25ppm	24.7		25ppm	0.342	24.36	98.62	
25ppm	24.81		25ppm	0.399	24.41	98.39	
50ppm	48.89	49.48	50ppm	6.091	42.80	87.54	89.40
50ppm	49.61		50ppm	5.236	44.37	89.45	
50ppm	49.93		50ppm	4.381	45.55	91.23	
100ppm	98.45	99.34	100ppm	46.89	51.56	52.37	53.48
100ppm	99.67		100ppm	44.28	55.39	55.57	
100ppm	99.89		100ppm	47.46	52.43	52.49	
250ppm	249.82	249.67	250ppm	187.1	62.72	25.11	25.43
250ppm	249.67		250ppm	184.3	65.37	26.18	
250ppm	249.51		250ppm	187.1	62.41	25.01	

B

Controls	Concentration	Average	Sample	Concentration	mg/L Bound	%Bound	Percent Bound
5 ppm	4.97		5 ppm	0.232	4.74	95.33	
5 ppm	5.03		5 ppm	0.254	4.78	94.95	
5 ppm	5.01	5.00	5 ppm	0.243	4.77	95.15	95.14
10 ppm	9.65		10 ppm	0.605	9.05	93.73	
10 ppm	9.76		10 ppm	0.78	8.98	92.01	
10 ppm	9.73	9.71	10 ppm	0.615	9.12	93.68	93.14
25ppm	24.4		25ppm	10.29	14.11	57.83	
25ppm	24.67		25ppm	10.46	14.21	57.60	
25ppm	24.56	24.54	25ppm	6.913	17.65	71.85	57.71
50ppm	49.67		50ppm	24.91	24.76	49.85	
50ppm	49.64		50ppm	27.35	22.29	44.90	
50ppm	49.74	49.68	50ppm	29.37	20.37	40.95	45.24
100ppm	98.94		100ppm	73.39	25.55	25.82	
100ppm	98.65		100ppm	73.35	25.30	25.65	
100ppm	98.89	98.83	100ppm	76.6	22.29	22.54	24.67
250ppm	249.87		250ppm	224.6	25.27	10.11	
250ppm	249.64		250ppm	219.6	30.04	12.03	
250ppm	249.91	249.81	250ppm	222	27.91	11.17	11.10

C

Controls	Concentration	Average	Sample	Concentration	mg/L Bound	%Bound	Percent Bound
5 ppm	4.97		5 ppm	2.600	2.37	47.69	
5 ppm	4.86		5 ppm	2.490	2.37	48.77	
5 ppm	4.89	4.91	5 ppm	2.760	2.13	43.56	46.67
10 ppm	9.82		10 ppm	4.7	5.12	52.14	
10 ppm	9.76		10 ppm	3.92	5.84	59.84	
10 ppm	9.78	9.79	10 ppm	4.77	5.01	51.23	54.40
25ppm	24.73		25ppm	20.51	4.22	17.06	
25ppm	24.67		25ppm	20.81	3.86	15.65	
25ppm	24.56	24.65	25ppm	21.13	3.43	13.97	16.36
50ppm	49.67		50ppm	42.59	7.08	14.25	
50ppm	49.56		50ppm	42.61	6.95	14.02	
50ppm	49.58	49.60	50ppm	43.23	6.35	12.81	13.70
100ppm	98.85		100ppm	92.25	6.60	6.68	
100ppm	98.58		100ppm	92.16	6.42	6.51	
100ppm	98.83	98.75	100ppm	92.36	6.47	6.55	6.58
250ppm	248.25		250ppm	244.7	3.55	1.43	
250ppm	249.23		250ppm	241.6	7.63	3.06	
250ppm	251.23	249.57	250ppm	244	7.23	2.88	2.46

APPENDIX B

Effect of solution pH: (A) As (III) (B) As (V)

A

Controls	Concentration	Average C.	Samples	Concentration	mg/L bound	% bound	Ave. % bound
pH 2 C	8.60	8.650	pH 2 S	5.87	2.78	32.13	31.143309
pH 2 C	8.66		pH 2 S	6.07	2.58	29.81	
pH 2 C	8.69		pH 2 S	5.93	2.72	31.49	
pH 3 C	8.74	8.859	pH 3 S	4.64	4.22	47.59	46.274834
pH 3 C	8.92		pH 3 S	5.03	3.83	43.19	
pH 3 C	8.92		pH 3 S	4.60	4.26	48.05	
pH 4 C	10.20	10.072	pH 4 S	4.24	5.83	57.90	57.904491
pH 4 C	10.19		pH 4 S	4.15	5.92	58.79	
pH 4 C	9.83		pH 4 S	4.33	5.74	57.02	
pH 5 C	8.74	8.789	pH 5 S	4.09	4.70	53.50	56.902829
pH 5 C	8.79		pH 5 S	3.89	4.90	55.78	
pH 5 C	8.84		pH 5 S	3.39	5.40	61.43	
pH 6 C	8.88	9.145	pH 6 S	4.90	4.25	46.44	51.587388
pH 6 C	9.65		pH 6 S	3.90	5.25	57.39	
pH 6 C	8.91		pH 6 S	4.49	4.66	50.93	

Controls	Concentration	Average C.	Samples	Concentration	mg/L bound	% bound	Ave. % bound
pH 2 C	10.170	10.193	pH 2 S	0.802	9.3913	92.13211	90.788097
pH 2 C	10.180		pH 2 S	1.103	9.0903	89.17920	
pH 2 C	10.230		pH 2 S	0.912	9.2813	91.05298	
pH 3 C	11.360	11.347	pH 3 S	3.648	7.6987	67.84959	68.666275
pH 3 C	11.340		pH 3 S	3.699	7.6477	67.40012	
pH 3 C	11.340		pH 3 S	3.319	8.0277	70.74912	
pH 4 C	10.780	10.777	pH 4 S	7.811	2.9657	27.51933	27.726570
pH 4 C	10.830		pH 4 S	7.447	3.3297	30.89700	
pH 4 C	10.720		pH 4 S	8.108	2.6687	24.76338	
pH 5 C	10.980	11.017	pH 5 S	9.233	1.7837	16.19062	16.605144
pH 5 C	10.950		pH 5 S	9.379	1.6377	14.86536	
pH 5 C	11.120		pH 5 S	8.950	2.0667	18.75946	
pH 6 C	11.160	11.137	pH 6 S	9.343	1.7937	16.10596	16.025142
pH 6 C	11.170		pH 6 S	9.102	2.0347	18.26998	
pH 6 C	11.080		pH 6 S	9.611	1.5257	13.69949	

Effect of solution pH on unmagnetized biochar: (A) As (III) (B) As (V)

A

Controls	Concentration	Average C.	Samples	Concentration	mg/L bound	% bound	Ave. % bound
pH 2 C	8.82	8.82	pH 2 S	8.83	-0.01	-0.10	-0.067994
pH 2 C	8.83		pH 2 S	8.83	0.00	-0.05	
pH 2 C	8.82		pH 2 S	8.83	0.00	-0.05	
pH 3 C	9.01	8.95	pH 3 S	9.02	-0.07	-0.76	-0.301676
pH 3 C	8.96		pH 3 S	9.01	-0.06	-0.69	
pH 3 C	8.88		pH 3 S	8.90	0.05	0.55	
pH 4 C	9.59	9.62	pH 4 S	9.59	0.02	0.23	-0.062402
pH 4 C	9.63		pH 4 S	9.64	-0.03	-0.27	
pH 4 C	9.62		pH 4 S	9.63	-0.01	-0.15	
pH 5 C	8.64	8.65	pH 5 S	8.81	-0.16	-1.83	-1.795761
pH 5 C	8.65		pH 5 S	8.81	-0.15	-1.79	
pH 5 C	8.66		pH 5 S	8.80	-0.15	-1.77	
pH 6 C	8.87	8.89	pH 6 S	8.87	0.01	0.17	0.030001
pH 6 C	8.90		pH 6 S	8.90	-0.01	-0.15	
pH 6 C	8.90		pH 6 S	8.88	0.01	0.08	

B

Controls	Concentration	Average C.	Samples	Concentration	mg/L bound	% bound	Ave. % bound
pH 2 C	10.75	10.780	pH 2 S	10.92	-0.1400	-1.29870	-1.267780
pH 2 C	10.82		pH 2 S	10.93	-0.1500	-1.39147	
pH 2 C	10.77		pH 2 S	10.90	-0.1200	-1.11317	
pH 3 C	11.05	11.063	pH 3 S	11.17	-0.1067	-0.96415	-0.662850
pH 3 C	11.06		pH 3 S	11.13	-0.0667	-0.60259	
pH 3 C	11.08		pH 3 S	11.11	-0.0467	-0.42181	
pH 4 C	10.88	10.830	pH 4 S	10.96	-0.1300	-1.20037	-0.831025
pH 4 C	10.83		pH 4 S	10.92	-0.0900	-0.83102	
pH 4 C	10.78		pH 4 S	10.88	-0.0500	-0.46168	
pH 5 C	11.01	10.977	pH 5 S	11.08	-0.1033	-0.94139	-3.552991
pH 5 C	10.97		pH 5 S	11.03	-0.0533	-0.48588	
pH 5 C	10.95		pH 5 S	11.99	-1.0133	-9.23170	
pH 6 C	11.14	11.120	pH 6 S	11.11	0.0100	0.08993	0.089928
pH 6 C	11.10		pH 6 S	11.06	0.0600	0.53957	
pH 6 C	11.12		pH 6 S	11.16	-0.0400	-0.35971	

Adsorption isotherms: (A) As (III) (B) As (V)

A

Controls	Concentration	Average	Sample	Concentration	mg/L Bound	%Bound	Percent Bound
5 ppm	4.76		5 ppm	2.326	2.44	51.17	
5 ppm	4.64		5 ppm	2.264	2.37	51.15	
5 ppm	4.67	4.69	5 ppm	2.932	1.74	37.27	46.53
10 ppm	9.165		10 ppm	5.272	3.89	42.48	
10 ppm	9.177		10 ppm	3.899	5.28	57.51	
10 ppm	9.176	9.17	10 ppm	3.895	5.28	57.55	52.51
25ppm	23.99		25ppm	12.49	11.50	47.94	
25ppm	23.08		25ppm	12.25	10.83	46.92	
25ppm	23.08	23.38	25ppm	12.32	10.76	46.62	47.43
50ppm	45.74		50ppm	30.96	14.78	32.31	
50ppm	45.64		50ppm	32.05	13.59	29.78	
50ppm	45.77	45.72	50ppm	32.1	13.67	29.87	30.65
70 ppm	63.38		70 ppm	46.54	16.84	26.57	
70ppm	63.76		70ppm	45.38	18.38	28.83	
70 ppm	63.57	63.57	70 ppm	46.08	17.49	27.51	27.64
100ppm	90.11		100ppm	72.83	17.28	19.18	
100ppm	90.97		100ppm	72.68	18.29	20.11	
100ppm	90.15	90.41	100ppm	72.23	17.92	19.88	19.72

B

Controls	Concentration	Average	Sample	Concentration	mg/L Bound	%Bound	Percent Bound
5 ppm	5.72		5 ppm	0.440	5.28	92.31	
5 ppm	5.75		5 ppm	0.440	5.31	92.35	
5 ppm	5.69	5.72	5 ppm	0.430	5.26	92.44	92.37
10 ppm	10.89		10 ppm	1	9.89	90.82	
10 ppm	10.71		10 ppm	0.959	9.75	91.05	
10 ppm	10	10.53	10 ppm	0.843	9.16	91.57	91.14
25ppm	26.39		25ppm	10.17	16.22	61.46	
25ppm	26.6		25ppm	10.36	16.24	61.05	
25ppm	26.57	26.52	25ppm	10.14	16.43	61.84	61.26
50ppm	51.36		50ppm	32.55	18.81	36.62	
50ppm	51.58		50ppm	32.47	19.11	37.05	
50ppm	51.71	51.55	50ppm	31.36	20.35	39.35	37.68
70 ppm	68.63		70 ppm	48.73	19.90	29.00	
70ppm	69.56		70ppm	49.08	20.48	29.44	
70 ppm	69.52	69.24	70 ppm	49.25	20.27	29.16	29.20
100ppm	103.1		100ppm	82.06	21.04	20.41	
100ppm	102.9		100ppm	81.87	21.03	20.44	
100ppm	102.8	102.93	100ppm	82.87	19.93	19.39	20.08

BIOGRAPHICAL SKETCH

Sergio Mireles was born 1993 in McAllen, Texas. He received the Bachelor of Science in Environmental Science from The University of Texas Pan American in 2015. He enrolled as a masters student in the School of Earth, Environmental, and Marine Sciences at the University of Texas Rio Grande Valley in 2015. His research, under the direction of Dr. Jihoon Kang, focused on using biochar as a low cost adsorbent for the removal of heavy metal from aqueous solution. He has published one peer reviewed article in the Journal of Earth Sciences & Environmental Studies. He received his MS in Agriculture, Environmental, and Sustainability Sciences in July 2017. Email: sergio.mireles01@utrgv.edu